
Masters Theses

Student Theses and Dissertations

Spring 2015

A new technique for modeling the geomorphology of a slow moving, soft-slope landslide using terrestrial LiDAR

Nathan Bradley Rohrbaugh

Follow this and additional works at: https://scholarsmine.mst.edu/masters_theses



Part of the [Geological Engineering Commons](#), [Geomorphology Commons](#), and the [Remote Sensing Commons](#)

Department:

Recommended Citation

Rohrbaugh, Nathan Bradley, "A new technique for modeling the geomorphology of a slow moving, soft-slope landslide using terrestrial LiDAR" (2015). *Masters Theses*. 7413.
https://scholarsmine.mst.edu/masters_theses/7413

This thesis is brought to you by Scholars' Mine, a service of the Missouri S&T Library and Learning Resources. This work is protected by U. S. Copyright Law. Unauthorized use including reproduction for redistribution requires the permission of the copyright holder. For more information, please contact scholarsmine@mst.edu.

A NEW TECHNIQUE FOR MODELING THE GEOMORPHOLOGY OF A SLOW
MOVING, SOFT-SLOPE LANDSLIDE USING TERRESTRIAL LIDAR

by

NATHAN BRADLEY ROHRBAUGH

A THESIS

Presented to the Faculty of the Graduate School of the
MISSOURI UNIVERSITY OF SCIENCE AND TECHNOLOGY

In Partial Fulfillment of the Requirements for the Degree

MASTER OF SCIENCE IN GEOLOGICAL ENGINEERING

2015

Approved by

Norbert Maerz, Advisor
J. David Rogers
Leslie Gertsch

ABSTRACT

Soft slope movement is a big problem whether it involves an engineered slope, one that is near infrastructure, or both. Active landslides that fail slowly sometimes allow ample time to affect remedial works. In order to plan effective remedial works, there needs to be a model of the entire geometry of the slide. This thesis describes a new approach to evaluate the morphology of slope geometry using Light Detection and Ranging (LiDAR) data obtained from simple targets strategically positioned on a slide body. The data was gathered in three-month intervals over a period of one year to allow enough time for any movement. Each scan produced tens of millions of points allowing a very detailed image to be used for processing.

Proprietary research code was developed at Missouri University of Science and Technology to manipulate LiDAR point-cloud data and further modified to interpret the data gathered for this thesis. The code uses a mesh system that the scan data is transformed to match. The mesh system is nothing more than a grid onto which the data is projected and it allows the follow-up programs to reference specific cells easier.

A minor amount of movement was detected over the course of a year and was consistent with what is expected for this type of landslide given the weather conditions for the year it was monitored. Furthermore, the calculated displacement is reasonably comparable to what was observed during ground-truthing. This process can be further enhanced to be useful in real-time monitoring of landslide hazard zones and allow for better mitigation (and less litigation) in the future. A detailed set of instructions are included in case this research should need to be reproduced or investigated further.

ACKNOWLEDGMENTS

This thesis would have never come to fruition had it not been for some very important people in both the author's personal and professional life. Dr. Norbert Maerz provided the necessary feedback and support, when it was needed most. Dr. Maerz made sure that the author was always gainfully employed and had the funding to do so. From his initial campus visit to the completion of a Master's and Second Bachelor's in Geological Engineering the author has Dr. Maerz to thank for the extra push to get things finished. The author will always be indebted to the support and candidness of his advisor, Dr. Maerz.

The author must also express his endless gratitude to his committee members Dr. J. David Rogers and Dr. Leslie Gertsch for their willingness to lend an ear and friendly advice. Both Dr. Rogers and Dr. Gertsch often gave the author a sanity check when it seemed like things were spiraling out of control. Each committee member provided their own unique, professional perspective to any question the author would bring them.

It should also be noted that this research would not have been possible had it not been for the expertise of Ken Boyko. Ken provided tireless effort to debug the research software and offered helpful ideas to make the data manipulation go smoother. His help allowed the author to get just a little more sleep at night.

The author would also like to thank his parents, Brad and Jessie, for always offering an extra boost of encouragement. The author is also thankful for his girlfriend, Laura, who provided endless support and served as a constant reminder that quitting is not an option. For the invaluable assistance from the Sentinels of Freedom Scholarship Foundation, the author is eternally grateful. Lastly, the author must recognize his peers, James, Kerry, Travis, Abdullah, and Kaba for facilitating a creative learning environment and providing an occasional laugh to relieve some stress.

TABLE OF CONTENTS

	Page
ABSTRACT.....	iii
ACKNOWLEDGMENTS	iv
LIST OF ILLUSTRATIONS.....	viii
LIST OF TABLES.....	x
 SECTION	
1. INTRODUCTION.....	1
1.1. OBJECTIVES	1
1.2. THESIS ORGANIZATION.....	1
2. BACKGROUND INFORMATION.....	3
2.1. SLOPE MOVEMENT	3
2.1.1. Types Of Slope Failure.....	3
2.1.1.1. Debris slump.....	6
2.1.1.2. Debris slide.	6
2.1.1.3. Earth slump.....	7
2.1.1.4. Earth slide.	8
2.1.1.5. Updated varnes' classification system.....	9
2.2. LIDAR TECHNOLOGY	9
2.2.1. Time-of-Flight.....	10
2.2.2. Phase Shift.	10
2.2.3. Comparison.....	10
2.3. POINT DATA.....	11
2.3.1. Point Cloud.	11
2.3.2. Floating Points.	12
2.3.3. Control Points.	12
2.3.4. Registration.....	13
2.4. RELEVANT RESEARCH.....	14

3. METHODOLOGY	17
3.1. SITE SELECTION	17
3.2. DATA ACQUISITION.....	20
3.3. EQUIPMENT	20
3.4. BOUNDARY CONDITIONS	21
3.5. EXPORTING DATA.....	22
3.6. PROCESSING ACQUIRED DATA	22
3.6.1. Procesing Software.	23
3.6.1.1. Findminmax.	23
3.6.1.2. Load.....	23
3.6.1.3. View2surf.....	23
3.6.1.4. Clipspheres.....	24
3.6.1.5. Findspheres.	24
3.6.1.6. Regballs.....	24
3.6.1.7. Surf2vrml.	24
3.7. BACKGROUND PROCESSING ENVIRONMENT.....	25
3.8. DIRECTORY	25
3.9. PARAMETERS	25
3.10. DISPLACEMENT PRECISION	27
3.10.1. Displacement Repeatability Test.	28
3.10.2. Precision Using the Incremental Displacement Apparatus.....	30
4. FINDINGS AND CONCLUSION.....	33
4.1. DATA	33
4.1.1. Point Files.	33
4.2. DISPLACEMENT VECTORS.....	40
4.3. SOURCES OF ERROR	35
4.4. RESULTS	35
4.5. SUGGESTIONS FOR IMPROVEMENT	39
4.6. CONCLUSION.....	40
APPENDICES	
A. SYSTEMATIC INSTRUCTIONS FOR GATHERING DATA.....	41

B. RESEARCH CODE.....	46
C. DATA TABLES	50
BIBLIOGRAPHY.....	59
VITA	61

LIST OF ILLUSTRATIONS

	Page
Figure 2.1 Movement Types	5
Figure 2.2 Debris Slump	6
Figure 2.3 Debris Slide	7
Figure 2.4 Earth Slump	8
Figure 2.5 Earth Slide along Table Rock Lake	9
Figure 2.6 Time-of-Flight and Phase Shift Principles	11
Figure 2.7 Up-Close Image of an Example Control Point	13
Figure 3.1 Map Showing Site Location in Relation to Rolla, Missouri	17
Figure 3.2 Research Site As Seen From Scanner Location in Summer	18
Figure 3.3 Research Site As Seen From Scanner Location in Winter	19
Figure 3.4 Transverse Tension Cracks in the Head	19
Figure 3.5 Site Being Mowed	20
Figure 3.6 Leica ScanStation2 Scanning At Site	21
Figure 3.7 Example Floating Point	23
Figure 3.8 A Screen Capture of the Point Labeling Process in View2Surf	24
Figure 3.9 Resolution File	27
Figure 3.10 Photo of Scan Site at Fraternity Circle	29
Figure 3.11 Real-World Simulation Scans at Fraternity Circle	29
Figure 3.12 Image of Incremental Displacement Apparatus	31
Figure 3.13 Example Scan of Apparatus	32
Figure 4.1 Movement of Floating Points That Penetrate Shear Plane	34
Figure 4.2 Movement of Floating Points That Do Not Penetrate the Shear Plane	34
Figure 4.3 Example Grid View of Site Showing Displacement	36
Figure 4.4 Reference Image Showing Location for Figures 4.5, 4.6 and 4.9	36
Figure 4.5 Example of a Rotated View of Site Showing Displacement between March and May	37
Figure 4.6 Displacement Spheres Attached to the Projected Bottom of Each Rod at the Middle Right Section of Site	37
Figure 4.7 Graphical Representation of Vectors at Site Viewed From Scanner Location	38

Figure 4.8 Graphical Representation of Vectors	38
Figure 4.9 Profile View of Slide.....	39

LIST OF TABLES

	Page
Table 2.1 Summary of Varnes' Classification Scheme	4
Table 2.2 Comparison of 11 Different Scanner Models	15
Table 3.1 Rod Configuration File	25
Table 3.2 Ball Size Configuration File	26
Table 3.3 Results of Test 1 With No Movement	28
Table 3.4 Results From An Initial Test Run of The Incremental Displacement Apparatus.....	30

1. INTRODUCTION

Determining the movement of an active landslide has often been accomplished by the use of INSAR (Interferometric Synthetic Aperture Radar) (Jaboyedoff et al., 2012), Airborne and/or Terrestrial LiDAR (Morgenstern and Martin, 2008), photogrammetry (Bitelli et al., 2003), tachymetry (Prokop and Panholzer, 2009), tilt meters (Garcia et al., 2010), or some combination of the aforementioned utilities. The method this thesis describes uses only Terrestrial LiDAR and simple targets. The morphology of a landslide is determined by comparing consecutive LiDAR scans to each other and calculating the displacement and direction of each target on the slide body. A sphere-finding algorithm was used to eliminate any potential interference like cars, vegetation, or insects.

The advantage the method introduced in this thesis has over other methods is its economy mixed with practicality. The field setup is minimal and cost effective while the data collection is routine and foolproof. The targets consist of ½-inch rebar with 4-inch Styrofoam balls emplaced with rebar chairs and silicon glue. The scanning location is a fixed point far enough away from the slide so as not to be influenced by any subsequent movement. The data gathered is very detailed and descriptive with sub-millimeter precision, in three dimensions. A typical scan day consists of about 30 individual scans lasting from 45 minutes to just over an hour. The resulting dataset consists of over 100 million data points. The frequency of scan visits is somewhat arbitrary, however, can be highly influenced by weather events.

1.1. OBJECTIVES

The objective of this research is to model the geomorphology of a slow-moving landslide using LiDAR and simple spherical targets by measuring the displacement and direction of the mathematical center of each sphere over a period of one year.

1.2. THESIS ORGANIZATION

This thesis is made up of four sections:

Section 1 introduces the thesis topic and outlines the overall objective of the thesis research.

Section 2 provides background information detailing types of soft slope movement and previous research using LiDAR and other techniques to monitor said movement.

Section 3 describes the methodology of the research and summarizes how/when the data was acquired as well as how it was processed in order to present the final product. Also included in Section 3 are details about site selection and specifics about the final site and setup conditions. At the end of Section 3 there is a description of some repeatability tests performed in order to substantiate the claims of sub-millimeter precision.

Section 4 presents the final product. The findings of a year's worth of research at the site and conclusions related to the methodology and thoughts on future advancements.

2. BACKGROUND

The research done for this thesis tries to re-introduce the idea of value engineering into a relatively costly method of slope modeling. Complexity does not make a favorable tool when a task must be completed by the standard layperson. Background research has revealed that, with time, the methods are only getting more complicated and apparently more costly. More pieces of equipment and high-tech tools are listed with each new publication. One of the underlying goals of this research was to come up with a simple method, using sophisticated equipment, to make high precision measurements of a landslide that someone completely unfamiliar could easily duplicate.

2.1. SLOPE MOVEMENT

Slope movement is generally categorized as one of the following: 1. Falls, 2. Topples, 3. Slides, 4. Spreads, or 5. Flows. Each category has an implicit reference to both the mode and speed of failure. It should be noted that both bedrock and soil comprise these five general categories. The scope of this thesis will focus on a specific texture of a specific type of movement: A rotational landslide containing more than 20% material coarser than sand that is slow moving. The entire research site is complex since it involves both rotational and translational movement; however, the general failure mode is rotational. While certain elements of the method described in this thesis may be applied to the other categories the focus will be on the type of landslide researched, a debris slump.

2.1.1. Types of Slope Failure. The terms used for soft slope movement can vary from one classification system to the next. The general definition of a landslide is a process that involves vertical and horizontal movement of soil, rock, or some combination of the two under the influence of gravity (Schuster, 1978). Landslides are largely grouped based on the size and properties of the material involved. Moreover, just like most areas of geology, there are many opinions on the specific classification. This thesis will utilize Varnes' classification scheme of 1978 for simplicity's sake (Varnes, 1978).

There are two types of slope movement of interest to this research: Slide, refers to translational sliding and Slump, refers to rotational sliding. Texturally, there are three main groups: Rock, Debris, and Earth. The term “Rock” refers to any part of bedrock. “Debris” is defined as a mixture of sand, gravel, cobbles, and boulders often with silt and clay. Earth is not well defined; however, Varnes defined debris as all material containing more than 20% sizes coarser than sand. From that, the definition of earth will be defined as all material containing less than 20% sizes coarser than sand. The types of land “slides” are then summarized as Debris/Earth Slide, or Debris/Earth Slump. Table 2.1 shows a summary of Varnes’ classification. Figure 2.1 shows a cartoon of the different movement types.

Table 2.1 Summary of Varnes’ Classification Scheme (Hung et al., 2013).

Movement type	Rock	Debris	Earth
Fall	1. Rock fall	2. Debris fall	3. Earth fall
Topple	4. Rock topple	5. Debris topple	6. Earth topple
Rotational sliding	7. Rock slump	8. Debris slump	9. Earth slump
Translational sliding	10. Block slide	11. Debris slide	12. Earth slide
Lateral spreading	13. Rock spread	—	14. Earth spread
Flow	15. Rock creep	16. Talus flow	21. Dry sand flow
		17. Debris flow	22. Wet sand flow
		18. Debris avalanche	23. Quick clay flow
		19. Solifluction	24. Earth flow
		20. Soil creep	25. Rapid earth flow
			26. Loess flow
Complex	27. Rock slide-debris avalanche	28. Cambering, valley bulging	29. Earth slump-earth flow

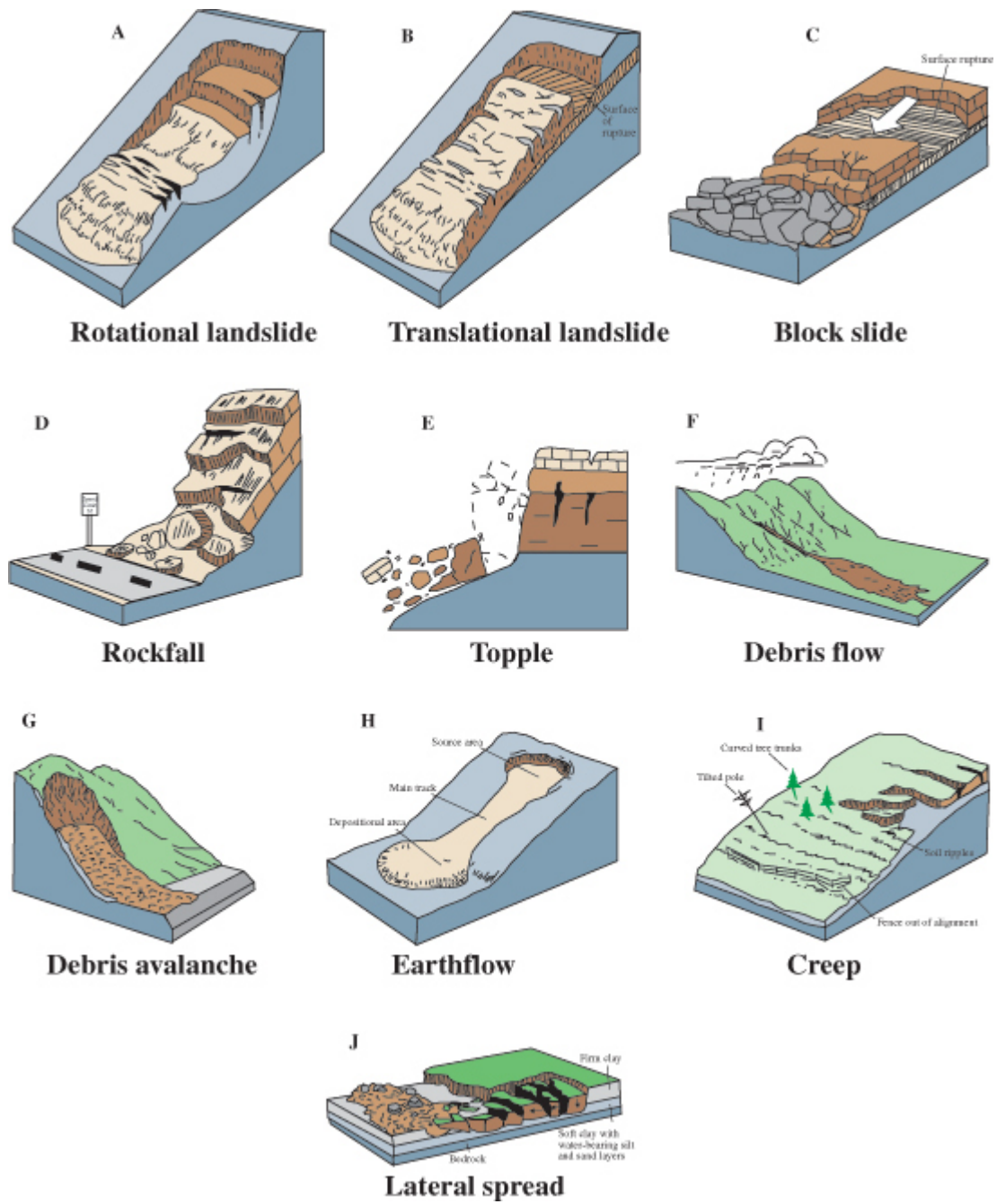


Figure 2.1 Movement Types (USGS, 2004-3072)

2.1.1.1. Debris slump. A debris slump is defined as a type of landslide where more than 20% of the material present is coarser than sand and is rotating. Figure 2.2 shows a cartoon of a debris slump.

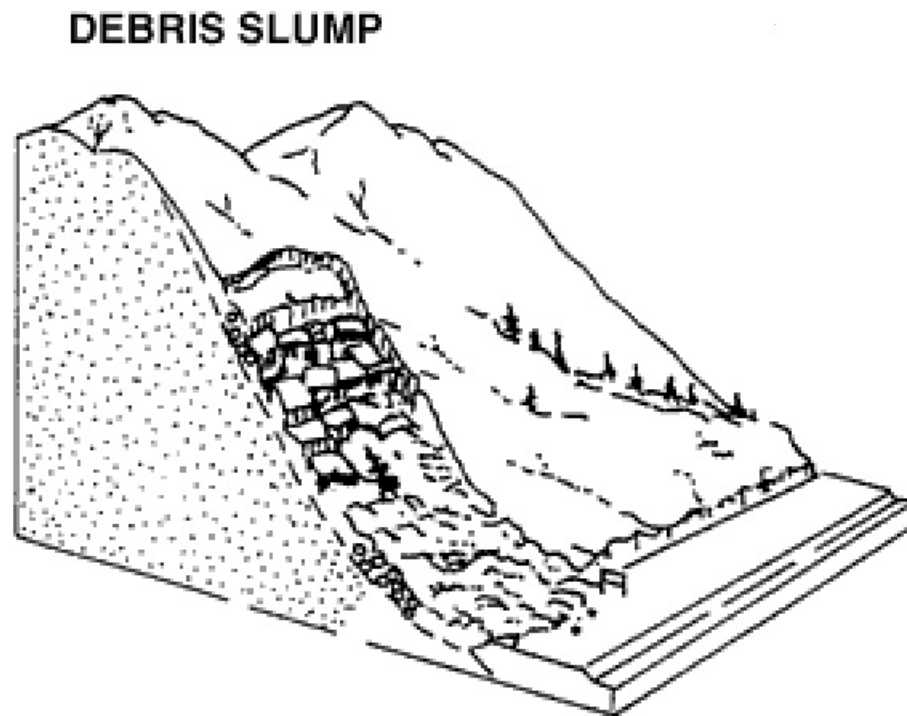


Figure 2.2 Debris Slump (After British Columbia Ministry of Forests, Lands, and Natural Resources)

2.1.1.2. Debris slide. A debris slide is defined as a type of landslide where more than 20% of the material present is coarser than sand and is translating. Figure 2.3 shows a cartoon of a debris slide.

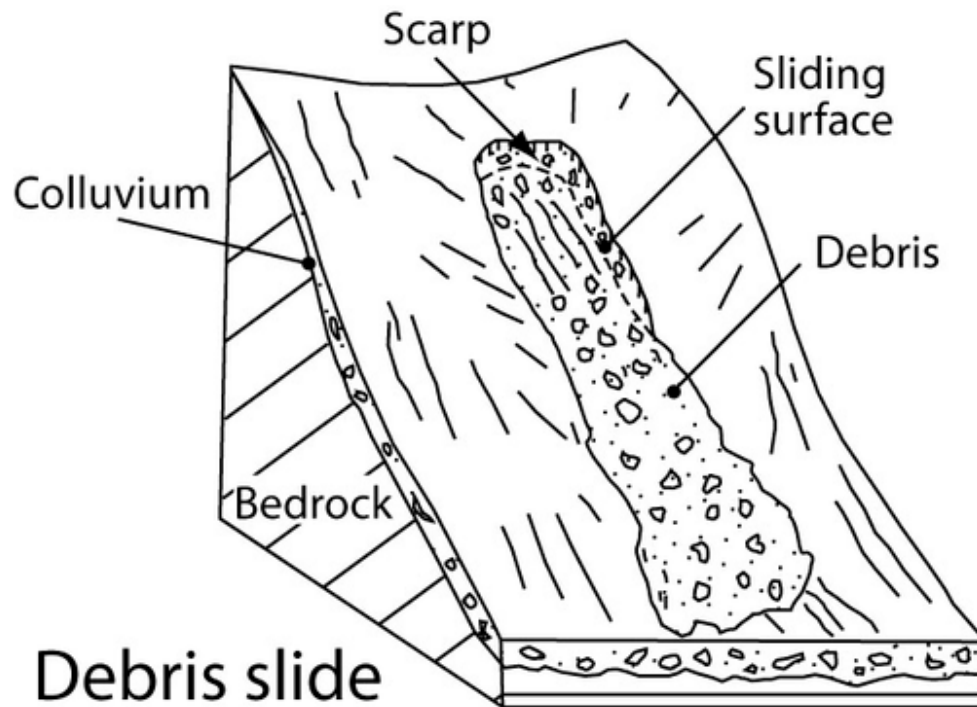


Figure 2.3 Debris Slide (Courtesy of University of Caen Lower Normandy)

2.1.1.3. Earth slump. An earth slump is defined as a type of landslide where less than 20% of the material present is coarser than sand and is rotating. Figure 2.4 shows a photo of an earth slump.

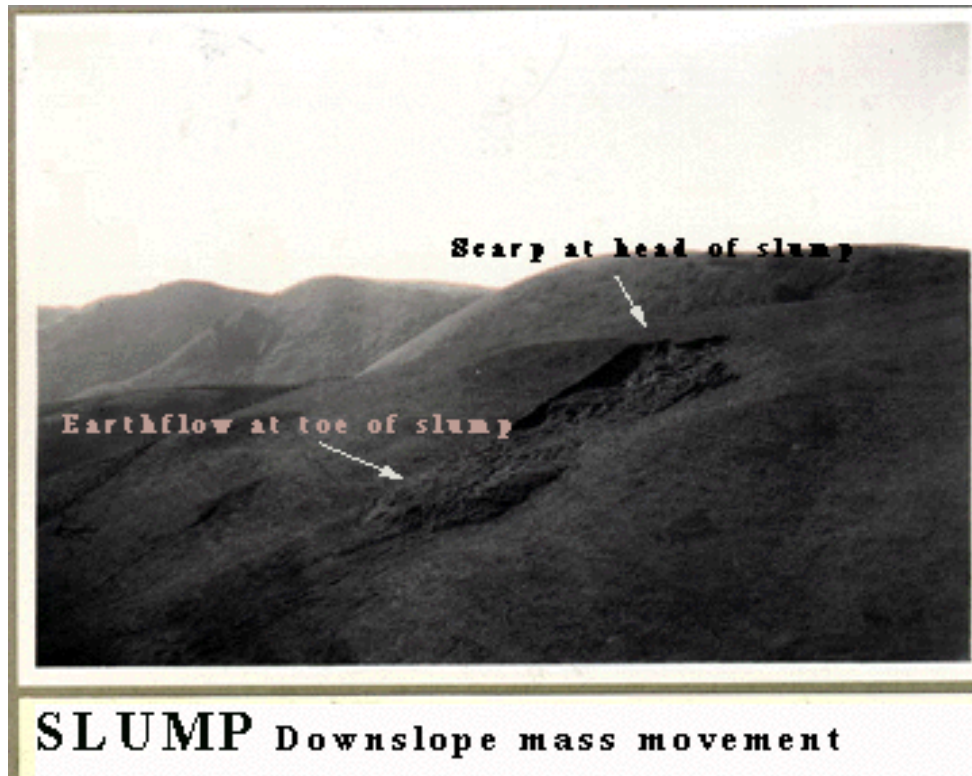


Figure 2.4 Earth Slump (Courtesy of United States Search and Rescue Task Force)

2.1.1.4. Earth slide. An earth slide is defined as a type of landslide where less than 20% of the material present is coarser than sand and is translating. Figure 2.5 shows an image of an earth slide at Table Rock Lake in southern Missouri.



Figure 2.5 Earth Slide along Table Rock Lake (USACE)

2.1.1.5. Updated varnes' classification. In their review of Varnes' Classification Scheme, and with respect to other authorities on the subject, Hungr et al. (2013) made some minor classification changes. It is sufficient to note that in their revision, they pointed out how Varnes' original classification did not have any implications toward plasticity of material. Had the focus of this thesis been on what causes the soft slope movement the updated Varnes' Classification would have been used.

2.2. LiDAR TECHNOLOGY

The technology used for this research is a relatively new tool. LiDAR (Light Detection and Ranging) uses a highly focused laser beam to collect data and construct a three-dimensional point cloud. LiDAR is a very proficient tool when used within its capabilities. Newer LiDAR scanners are being advertised as the fastest yet, but reality is most affordable scanners sacrifice resolution for speed. In the case of this research, reasonable scan times and a very high resolution were required. In this instance, newer was not better. This section will cover some of the most recent research using LiDAR, similar to that covered in this thesis, as well as general information about the functionality of LiDAR technology.

2.2.1. Time-of-Flight. The two predominant types of three-dimensional laser scanners are time-of-flight and phase shift. Both collect the same kind of data, but operate on different principles. Since the Leica ScanStation2 is a time-of-flight scanner that is what this paper will focus on. Time-of-flight scanners operate under the principle that light travels at a constant speed and based on the time of flight the scanner can calculate the distance to an object. The principle is governed by this simple equation:

$$\text{Distance} = \frac{\text{Speed of Light} \times \text{Time of Flight}}{2}$$

2.2.2. Phase Shift. Phase-shift scanners operate under the principle that when light is reflected from an object it changes phase ever so slightly. A sensor within the scanner compares the phase of the light emitted to that of the light reflected and then calculates the time-of-flight based on the following equation:

$$\text{Time of Flight} = \frac{\text{Phase Shift}}{2\pi \times \text{Modulation Frequency}}$$

2.2.3. Comparison. The two types of scanners gather the same data, but they do differ in certain respects. Figure 2.6 shows a comparison between time-of-flight and phase shift optics. For example, time-of-flight scanners are generally more reliable at scanning greater distances than phase shift scanners. This allows for scanning slopes from a safer distance without sacrificing quality. On the other hand, phase shift scanners can acquire data faster at close range and are sometimes preferred for confined spaces. When calculating the time a project will take from start to finish the two largest parts were often the scanning time and the post-processing time. The software created at Missouri S&T has all but eliminated the need to consider time as a significant factor. Prior to this research, the software could take more than an hour to process one large scan. After new steps were added to the research code processing rarely takes more than fifteen minutes.

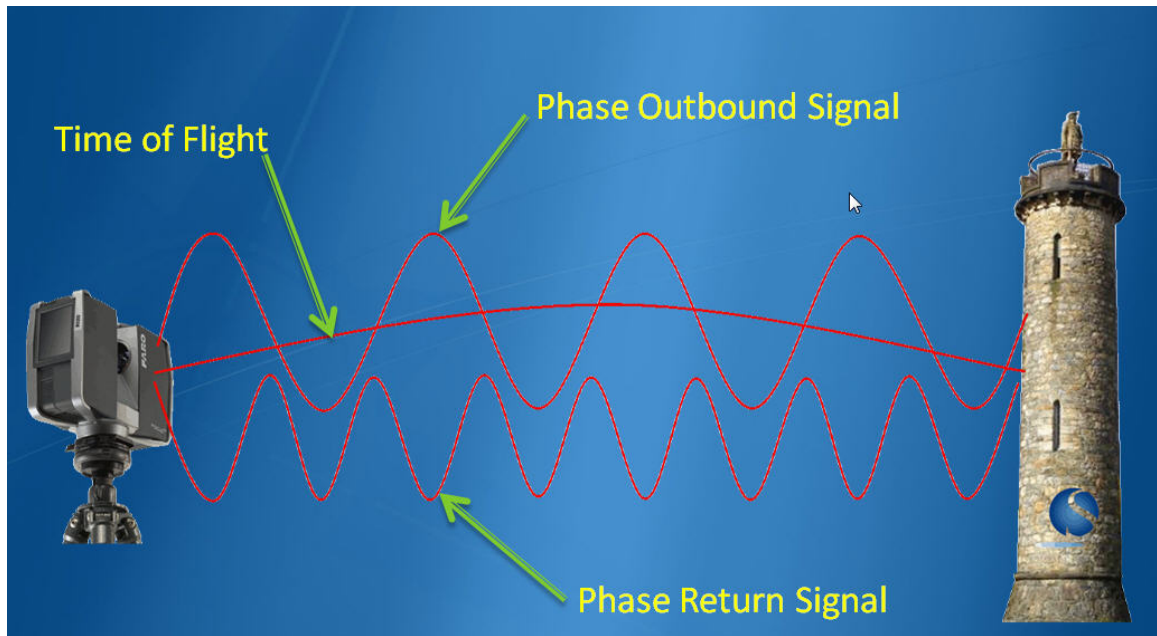


Figure 2.6 Time-of-Flight and Phase Shift Principles (SurvTech Solutions)

2.3. POINT DATA

When data is collected using the Leica ScanStation2 it is represented by a collection of points, referred to as a point cloud. A point cloud can contain a wealth of information, but the output format is dependent on the user's needs.

2.3.1. Point Cloud. Each point cloud represents a surface, which has reflected the laser beam back to the scanner. This surface is sometimes the true target area of interest and sometimes it is interrupted by objects that come between the scanner and the target area, such as birds, bugs, cars, vegetation, unruly bicyclists, etc. Each point that makes up the point cloud is given a specific value. The typical format comes in four flavors:

- XYZ format: a format that reports only a location in space with no extra information given
- XYZI format: a format that reports both the spatial location and intensity information
- XYZRGB format: a format that reports both the spatial location as well as the Red, Green, and Blue color values at each point

- XYZIRGB format: a format that reports the spatial location, intensity, and color information for each point

The software that records the raw scan data directly from the Leica ScanStation2, called Cyclone, is only useful for visualization and minor manipulation of the point clouds. Since the research software has limitations too, it is useful to minimize the amount of data exported from Cyclone. In Cyclone, the scene is rotated and clipped so that it can be exported in a point format. The research software is designed to handle only ASCII (American Standard Code for Information Interchange) type files. Properly preparing the point cloud in Cyclone allows for a seamless transition into the processing software, which will ensure accurate displacement measurements. Precision of the results depends on the movement of floating points and the lack of movement of control points.

2.3.2. Floating Points. The targets placed over the body of the slide were aptly named floating points. The targets were made up of varying lengths of rebar and two 4-inch Styrofoam balls, placed one foot apart. Using spheres as targets allows the processing software to ignore whether the scanner is perfectly level or the slope is exactly perpendicular to the scanner's line of sight. This built in feature gave the author freedom to scan from the same location each time and angle of incidence never played a role when displacement was calculated.

2.3.3. Control Points. The targets labeled as control points were made up of pieces of rebar and one 4-inch Styrofoam ball. Figure 2.7 shows an image of a control point. Each control target was strategically placed outside the influence of slope movement. Needing at least four control points to affect a usable transform, the author built redundancy into the design to maintain data integrity by installing ten. The control points were meant to be static throughout the duration of the research so that consecutive dates, as well as beginning and end dates, could be compared. Ten control targets were distributed along the outer edges of the scan area. Two of which were placed at each corner since this is where the largest source of distortion occurs.



Figure 2.7 Up-Close Image of an Example Control Point.

2.3.4. Registration. Probably the single most important part of this entire process is the registration. Registration is the process of taking a baseline scan and fitting all successive scans onto it. This is where the control points come into play. For each new scan date, the scanner may not be set up in the exact same position and the tribrach may have been adjusted since the last scan. All of these variables are null provided the control points have not been disturbed. In order to obtain the highest level of precision, the control points must not experience any type of movement. Great care was taken when setting up the site to make sure the control points would not be disturbed. Considering the amount of time that the site would be in use, the author decided to include redundancy in the design. The processing software required a minimum of three control points, but with 3-D data, four control points are the preferred minimum. The author installed ten control points in case something did not go as planned. The processing software compares all “after” scans back to the original base date scan and calculates a root mean square error (RMSE). The size of this error gives the user an idea of the precision of the displacement results.

2.4. RELEVANT RESEARCH

This section will highlight some recent research that assesses and uses the advanced capabilities of LiDAR to monitor or model soft slope movement. All of the papers discussed use a different approach than what this thesis covers and generally report less precision than research for this thesis produced.

Prokop and Panholzer (2009) did research to determine the reliability of terrestrial laser scanning (TLS). They analyzed their results by processing the data through ArcGIS 9.2 to produce high-resolution digital elevation models (HRDEM). The goal of their research was to determine how well a slow-moving landslide could be monitored. They defined slow moving as movement of a slope less than 100 millimeters per scanning date.

The Gallierm Landslide, in Vorarlberg, Austria, measured approximately 100 meters by 100 meters and was considered slow moving. To compare TLS measurement precision, the research team used tachymetry on the same reflective targets placed on a geodetic grid within the slide body. They also used natural targets, such as rocks, for points of reference. Given the limitations of their scanner, which was a Riegl LMS Z420i, and the processing technique they were unable to determine any movement less than 50 millimeters. The technique they used depended on a linear increase in laser beam width with distance.

According to Lichti and Jamtsho (2006), the ideal point spacing should measure no more than 86% of the beam width at the scanning distance. This constraint caused the research team to scan the entire site at a resolution of 3 centimeters at a distance of 100 meters. Table 2.2 shows a comparison of eleven different TLS systems and their capabilities at 50 meters.

Lichti and Jamtsho also used a highway surface as a planar feature to register point clouds. As noted in their paper, the highway proved to be a difficult target for picking identical control points. The research team used several techniques to produce the desired results, but most fell outside of their precision limitation.

Table 2.2 Comparison of 11 Different Scanner Models

<i>Make</i>	<i>Model</i>	Sampling Increment Δ (mm)	Beam Width δ (mm)	<i>EIFOV</i> (mm)	<i>EIFOV</i> / Δ
Callidus	CP 3200	54.5	232.0	205.6	3.8
Faro	LS 880	0.7	15.5	13.3	19
I-SiTE	4400	94.2	100	124.6	1.3
Leica	HDS 2500	0.25	6.0	5.2	21
Leica	HDS 3000	1.2	6.0	5.3	4.4
Optech	ILRIS-3D	1.0	20.5	17.6	18
Riegl	LMS-Z210	62.8	150.0	141.5	2.3
Riegl	LMS-Z210i	8.7	150.0	129.1	15
Riegl	LMS-Z420i	3.5	12.5	11.2	3.2
Trimble	GS200	1.6	3.0	3.0	1.9
Zoller and Frohlich	Imager 5003	15.7	14.0	19.4	1.2

Jaboyedoff et al. (2012) highlight the difficulties with scanning a highly vegetated slope. Often the need for more than one return or an intensive filtering method was cited. The difference in that research method is the type of targets used. Jaboyedoff's team tried to use natural features in the scene, which were often rocks. While edges and corners of rocks allow for reasonably small root mean square error (RMSE) in registration, there remains significant potential for human "picking" error. The likelihood of a person choosing the exact same spot on a rock from one scan to another is very low. The presence of vegetation only adds to the possibility of a "picking" deviation.

Gordon et al. (2003) researched what could be considered a precursor to the research presented in this thesis. Gordon's research team used TLS to detect structural deformation in wood and concrete with an array targets placed over each piece of test material. To establish an absolute coordinate system for the LiDAR, the team incorporated photogrammetry and targets scattered around the room. The research highlights some very important points that the author considered when performing the research for this thesis. Research results cannot claim to be more precise than the single point precision of the LiDAR unit that is doing the scanning unless there is some type of post-processing involved. The author would like to include that idea as a disclaimer to this thesis.

The results obtained by the research for this thesis are claimed to have sub-millimeter precision. The precision does not come solely from the ScanStation2. Leica Geosystems reports that the ScanStation2 has a point spacing capability of one millimeter through its full scanning range. Where the ability to obtain sub-millimeter precision comes from is the proprietary software developed at Missouri S&T. The software uses the raw data points to calculate the theoretical center of each sphere in the scene. These theoretical centers are then compared to “before” and “after” scans and that results in sub-millimeter precision.

3. METHODOLOGY

At the onset of this research project, the author was presented with four potential sites to study. The closest was 35 minutes east of Rolla, in Bourbon. The farthest was 2 hours and 15 minutes southwest of Rolla, in Branson. The remaining two were between an hour and 2 hours away, in Columbia, MO and Branson, MO, respectively. Figure 3.1 shows a map to the site used for this research.

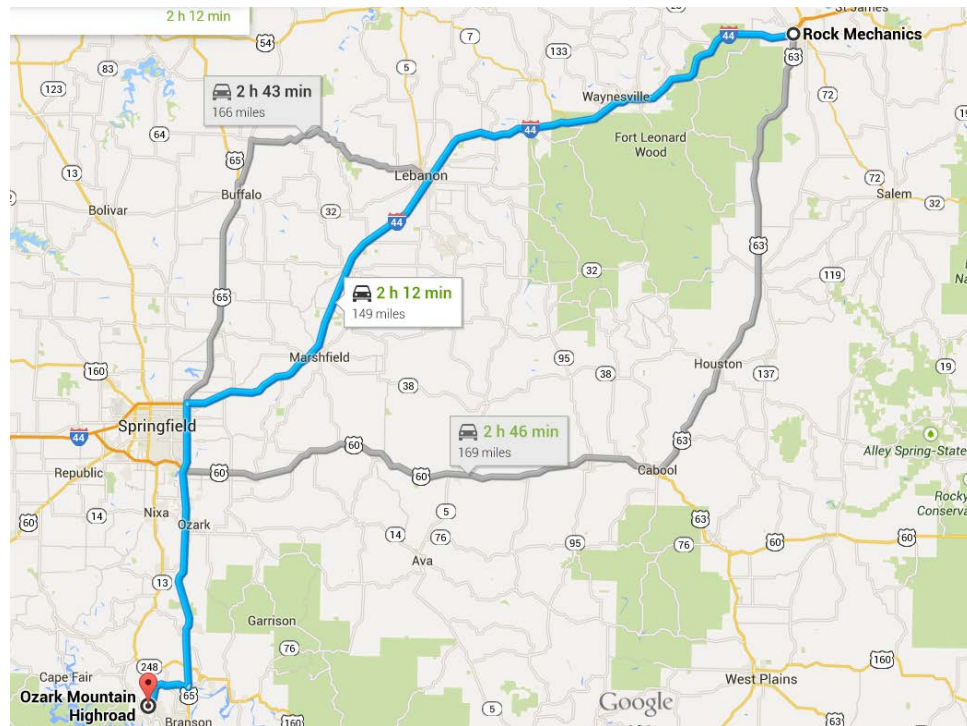


Figure 3.1 Map Showing Site Location in Relation to Rolla, Missouri

3.1. SITE SELECTION

The ideal conditions for scanning would include a safe, level scanning area and a slope 75 meters away that was nearly perpendicular to the laser eye. The ideal slope conditions would be a classic, textbook style slide that has uniform, predictable motion

and no hidden complications. The site used for this thesis falls somewhere less than ideal for both of the above parameters. The scanning area is on a slight grade, but it is at least safe and an average of 70 meters from the slide. The slope is the wildcard. It is approximately 60° from level, a traditional slump style movement mixed with several micro features to include rotational and translational slides within the slide body, and its movement lacks regularity. Figures 3.2-3.5 show the site used for this research.



Figure 3.2 Research Site As Seen From Scanner Location in Summer



Figure 3.3 Research Site As Seen From Scanner Location in Winter

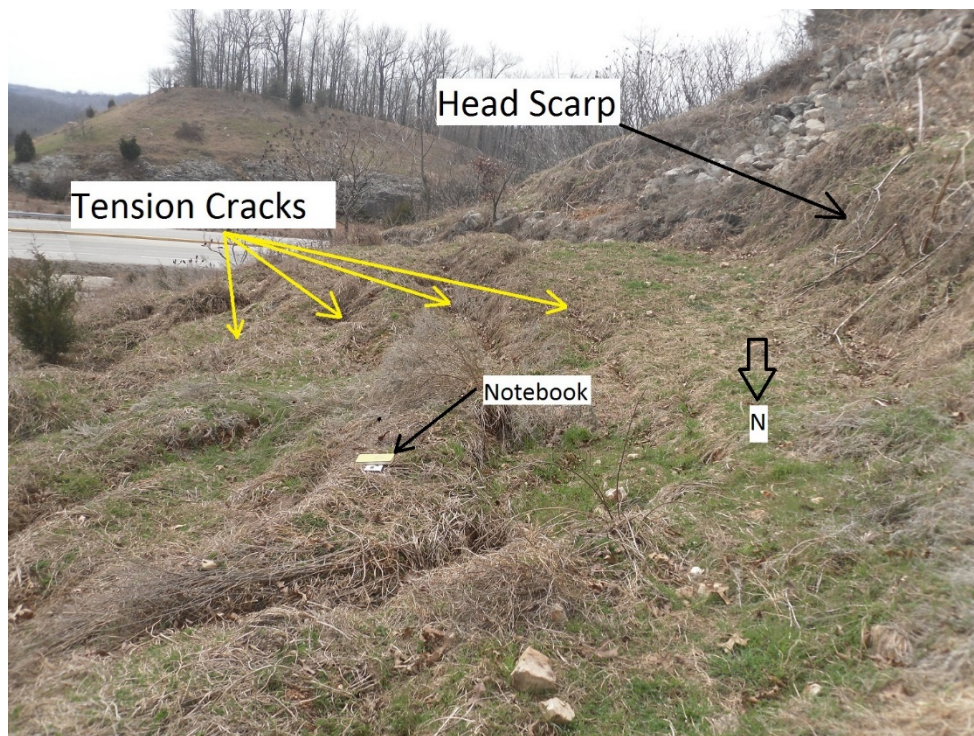


Figure 3.4 Transverse Tension Cracks in the Head (4.75"x7.5" Field Book for Scale)



Figure 3.5 Site Being Mowed (Author for Scale)

3.2. DATA ACQUISITION

The scanner settings were kept to a very tight regime for this research. Given the constraints by the processing software, the site had to be scanned in sections. The control points were scanned at the highest resolution of 1mm x 1mm. The floating points were scanned at 2mm x 2mm. A third scan was taken of the entire slide body at 5mm x 5mm, mainly for visualization purposes. Each scan was pinged using the points nearest the center of the scan window to get a proper estimate of the average distance.

3.3. EQUIPMENT

The equipment used came in a mixed bag. The author began this research using a FARO laser scanner, but later switched to the trusty Leica ScanStation2. Honda Eu1000i and Eu2000i generators were used as primary power sources. The secondary power source came in the form of an AC adapter working from the author's vehicle. An electric weed eater came in handy during the warmer months where vegetation was out of

control. ½-inch steel rebar, 4-inch Styrofoam balls, and silicon glue were used for the targets. Each piece of rebar came in 20-foot sections and had to be cut using both hand-held bolt cutters and a DeWalt Chop Saw. A Dell Laptop Workstation was used to gather and display the raw data points using Leica's Cyclone software. Figure 3.6 shows the equipment setup during scanning.

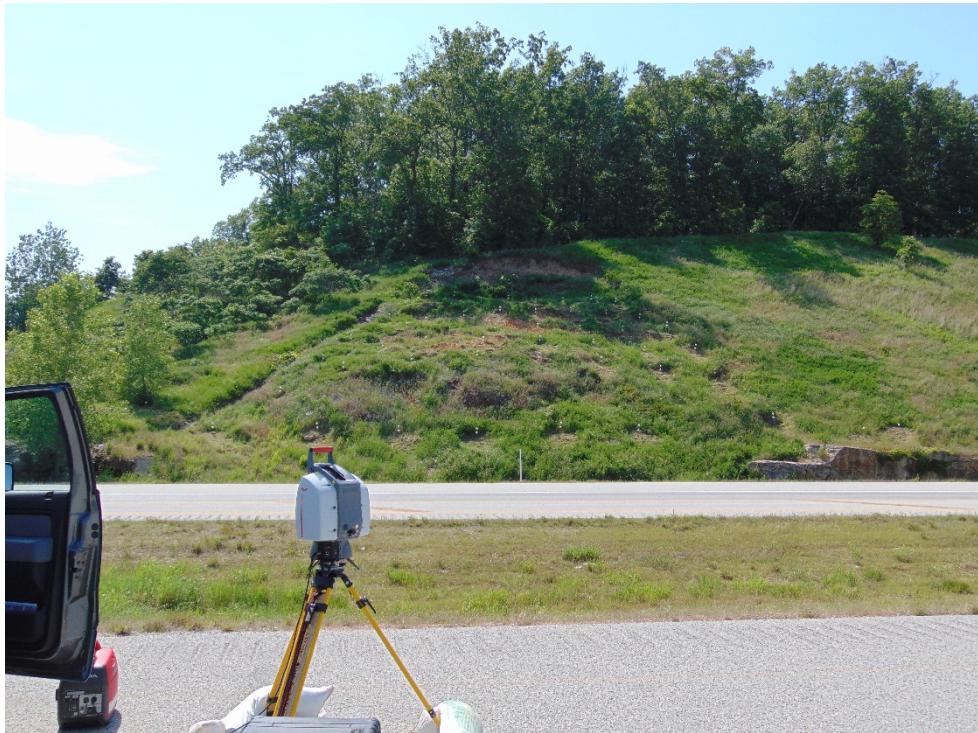


Figure 3.6 Leica ScanStation2 Scanning At Site

3.4. BOUNDARY CONDITIONS.

The Leica ScanStation2 User Guide suggests not using the scanner when outside temperatures are below 32°F. It must also be kept dry and shielded from continuous, direct sunlight. Another issue that came into play at this site was wind. The ScanStation2 weighs upwards of 40lbs. and sitting just over 4 feet off the ground, it is susceptible to strong wind gusts. The author placed 40lb. sandbags on each leg of the tripod to stabilize the scanner.

The site's measurements are 49 feet across the top, 101 feet across the bottom, 92 feet on the left side and 75 feet on the right side. The irregularity of the body did not allow for an even spacing of floating points. The spacing between floating points in the top row averaged 6ft/point. The second row averaged 8.5ft/point. The third row averaged 10ft/point. The fourth row averaged 12ft/point. The fifth row averaged 13ft/point. The sixth row averaged 14ft/point. The spacing floating points in each column followed a similar instance. From the far left column, the floating points averaged 18ft/point. The far right column averaged 12ft/point, except the bottom two points, which averaged 25ft/point.

3.5. EXPORTING DATA

Once the final scan was complete, the data was briefly analyzed at the site to make sure there were no blank spaces in the scene. The data was then taken to the office where it was prepared to match the format used by the processing software. The scene was trimmed to include only the required data points. The scene is then exported as a point file, in XYZIRGB format.

3.6. PROCESSING ACQUIRED DATA

The idea behind the spherical targets is to model movement of the slope without having to sift through the millions of points that cover the entire surface of the slide body. The control points consist of one sphere placed atop a piece of rebar. Since the control points are not expected to move, a second sphere is not required. Note is taken if any movement is noticed and the control point is rendered useless. The floating points are made up of two spheres spaced one foot apart on pieces of rebar that are three, four, or five feet in length. Each type of targets is then given a "role" of their respective purpose in the software, either a control role or a floating role. Figure 3.7 shows an example of a floating point. The software used to process the raw LiDAR point clouds was developed at Missouri S&T by Ken Boyko. It involves a combination of several programs that each performs a specific function. The software is set up with a mesh resolution of 35 millimeters and is programmed to allow more than one hit per pixel. This means that the scanner resolution at the site can be anything less than 35 millimeters and the data will

still work. When the data is first loaded into the program it is reconfigured into the 35-millimeter resolution with overall window constraints of 4300 pixels Horizontal x 3400 pixels Vertical.

3.6.1. Processing Software. The processing software used for this thesis research is a series of 7 C++ programs that run recursive algorithms. The user must initiate each command through the command module in DOS. The data is meshed, binned, sorted, clipped, and finally processed via each piece of software.

3.6.1.1. Findminmax. Finds the minimum and maximum range of x, y, z's in the point cloud so that a binary file can be set up correctly for the next program to be initiated.

3.6.1.2. Load. Reads the points file and bins all the points into a mesh predefined in a resolution configuration file.

3.6.1.3. View2surf. A step where duplicate images of the same scene are shown allowing the user to label each sphere with an ID and a role on the left screen while keeping an idea of general location on the right screen. Figure 3.8 shows an example of some points that have been given roles and ID's.

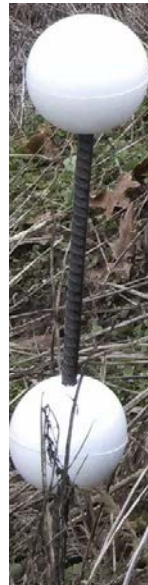


Figure 3.7 Example Floating Point

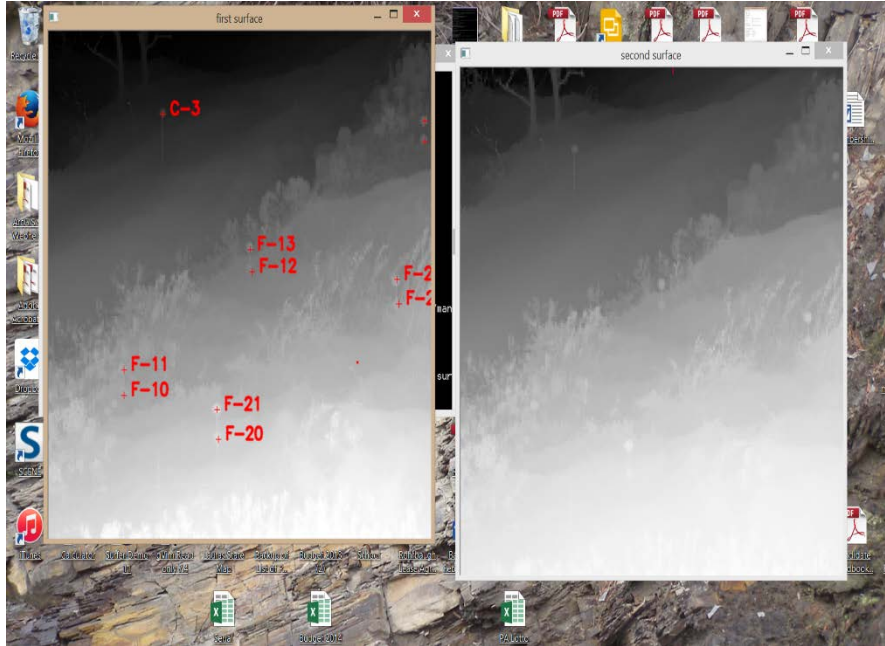


Figure 3.8 A Screen Capture of the Point Labeling Process in View2Surf

3.6.1.4. Clipspheres. The ClipSpheres function uses the “picked” points from the View2Surf program to eliminate any points in the scene that are not spheres. Occasionally, a stray piece of vegetation will be accidentally picked and this step will eliminate it. Typically, the ClipSpheres function will trim the original point file by 98%. This allows the rest of the process to go much faster.

3.6.1.5. Findspheres. Calculates the theoretical center of all spheres output from the previous program, ClipSpheres, using a recursive method.

3.6.1.6. Regballs. Uses the spheres labeled as control points to overlay consecutive scans with minimal root mean square error (RMSE). Each new date is compared to the “base” scan, which is generally the first scan date. The RMSE can be calculated for all before-after combinations.

3.6.1.7. Surf2vrml. Creates a VRML (Virtual Reality Modeling Language) model of the rods, spheres, and slope for visual examination.

3.7. BACKGROUND PROCESSING ENVIRONMENT

All software was developed in C++, compiled using GCC© (GNU compiler collection), and runs on Ubuntu© Linux. Two open-source libraries are used for graphic output – OpenCV (Open Source Computer Vision Library) for graphic output and OpenGL™ for interactive display functions (Ken Boyko, personal communication, 10 December 2014). This section describes how the processing is set up, including the directory structure, and parameter tuning.

3.8. DIRECTORY

The root directory for the processing was kept in the C:\ drive for ease of access. A skeleton template exists from the original software development and each time a new project is run that skeleton template is just copied into a folder named OutCropData. Most of the executable programs write log files that contain details of the processing steps. Each of the empty folders in the skeleton file is built to hold these processed files for later review, or should something go wrong during processing.

3.9. PARAMETERS

Several executable files are controlled by tuning configuration files, which control the behavior of that executable. The configurations files used for this thesis consisted of: RodConfig, BallSize, Resolution, and VRMLDateList. Tables 3.1 and 3.2 show an example of a rod configuration file and a ball size file. Figure 3.9 shows an example of a resolution configuration file.

Table 3.1 Rod Configuration File

Rod Above Ground (in)	24	Ball Radius (mm)	50.8				
Role	Ball ID	Ball ID	Total Rod Length	Role	Ball ID	Ball ID	Total Rod Length
c	1	1	4	f	44	45	5
c	2	2	4	f	46	47	3
c	3	3	4	f	48	49	4
c	4	4	4	f	50	51	5
c	5	5	4	f	52	53	5
c	102	102	4	f	54	55	5
c	103	103	4	f	56	57	3

Table 3.1 Rod Configuration File (Cont.)

c	104	104	4	f	58	59	4
f	6	7	4	f	60	61	5
f	8	9	5	f	62	63	3
f	10	11	3	f	64	65	4
f	12	13	4	f	66	67	3
f	14	15	5	f	68	69	4
f	16	17	3	f	70	71	5
f	18	19	5	f	72	73	3
f	20	21	3	f	74	75	4
f	22	23	4	f	76	77	5
f	24	25	3	f	80	81	5
f	26	27	4	f	82	83	3
f	28	29	5	f	84	85	4
f	30	31	3	f	86	87	5
f	32	33	4	f	88	89	3
f	34	35	5	f	90	91	5
f	36	37	3	f	92	93	3
f	38	39	4	f	94	95	4
f	40	41	5	f	96	97	5
f	42	43	4	f	98	99	3
				f	100	101	4

Table 3.2 Ball Size Configuration File

ID	Diameter	ID	Diameter	ID	Diameter
1	4	35	4	69	4
2	4	36	4	70	4
3	4	37	4	71	4
4	4	38	4	72	4
5	4	39	4	73	4
6	4	40	4	74	4
7	4	41	4	75	4
8	4	42	4	76	4
9	4	43	4	77	4
10	4	44	4	80	4
11	4	45	4	81	4
12	4	46	4	82	4
13	4	47	4	83	4
14	4	48	4	84	4
15	4	49	4	85	4

Table 3.2 Ball Size Configuration File (Cont.)

16	4	50	4	86	4
17	4	51	4	87	4
18	4	52	4	88	4
19	4	53	4	89	4
20	4	54	4	90	4
21	4	55	4	91	4
22	4	56	4	92	4
23	4	57	4	93	4
24	4	58	4	94	4
25	4	59	4	95	4
26	4	60	4	96	4
27	4	61	4	97	4
28	4	62	4	98	4
29	4	63	4	99	4
30	4	64	4	100	4
31	4	65	4	101	4
32	4	66	4	102	4
33	4	67	4	103	4
34	4	68	4	104	4

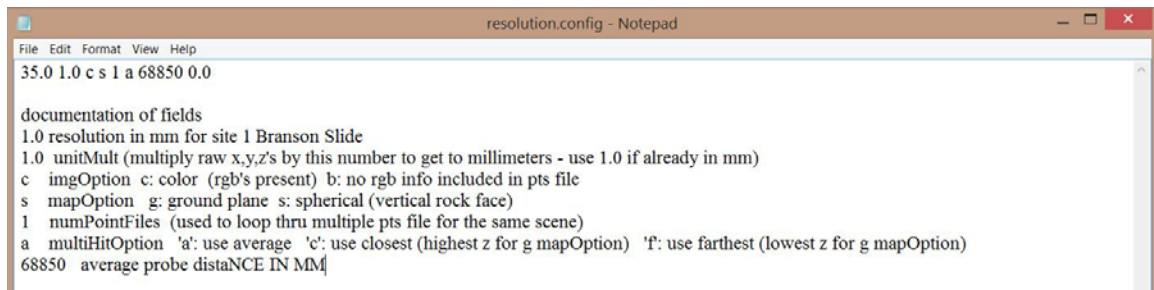


Figure 3.9 Resolution File

3.10. DISPLACEMENT PRECISION

One of the biggest concerns when processing the raw data is the precision. The author used a few different tests to ensure the greatest precision possible was being produced. The first test was composed of several sets of scans. Each set of scans simulated a different aspect of the scanning process that would occur at the research site.

3.10.1. Displacement Repeatability Test. A small slope near the soccer field at Fraternity Circle, in Rolla, was used to perform repeatability tests. Figure 3.10 is a photo of the test site. Targets were scanned at the same distance as at the field site. The displacement repeatability test was performed to see how well the processing software could place the control points of each scan. Table 3.3 shows the numerical results of the repeatability test. This brought to light the effect that not using the exact same scanning location had on the overall results. Several iterations of scans were taken to simulate different field problems. The first set of scans was taken with the targets and scanner remaining stationary between the before and after scans. The next set of scans involved moving the targets by pulling the rods forward and leaving the scanner in place between the before and after scans. The third set of scans was real-world simulation with the targets and scanner moved between the before and after scans. Figure 3.11 shows the results of the final displacement scan at the test site at Fraternity Circle in Rolla.

Table 3.3 Results of Test 1 With No Movement

Repeatability Test															
(all units mm)															
Observation 1				Observation 2											
ball ID	x	y	z	ball ID	x	y	z	dx	dy	dz	dx2	dy2	dz2	dist	avg dist
1	6171.86	56187.2	-168.646	1	6172.34	56186.2	-168.59	0.48	-1	0.056	0.2304	1	0.003136	1.110647	0.661206
2	6758.4	56053	-160.173	2	6759.02	56053.3	-160.236	0.62	0.3	-0.063	0.3844	0.09	0.003969	0.691642	
3	6162.01	56074.1	-715.333	3	6162.41	56073.8	-715.183	0.4	-0.3	0.15	0.16	0.09	0.0225	0.522015	
4	6751.52	55946.2	-715.055	4	6752.26	55946.5	-715.097	0.74	0.3	-0.042	0.5476	0.09	0.001764	0.799602	
5	6432.19	55962.1	-618.89	5	6432.57	55962.3	-618.933	0.38	0.2	-0.043	0.1444	0.04	0.001849	0.431566	
6	6442.79	55990.1	-442.858	6	6443.27	55990.4	-442.914	0.48	0.3	-0.056	0.2304	0.09	0.003136	0.568802	
7	6452.26	56019.3	-266.889	7	6452.77	56019.5	-266.97	0.51	0.2	-0.081	0.2601	0.04	0.006561	0.55377	
8	6462.91	56047.7	-92.0966	8	6463.48	56047.9	-92.1923	0.57	0.2	-0.0957	0.3249	0.04	0.009158	0.611603	



Figure 3.10 Photo of Scan Site at Fraternity Circle

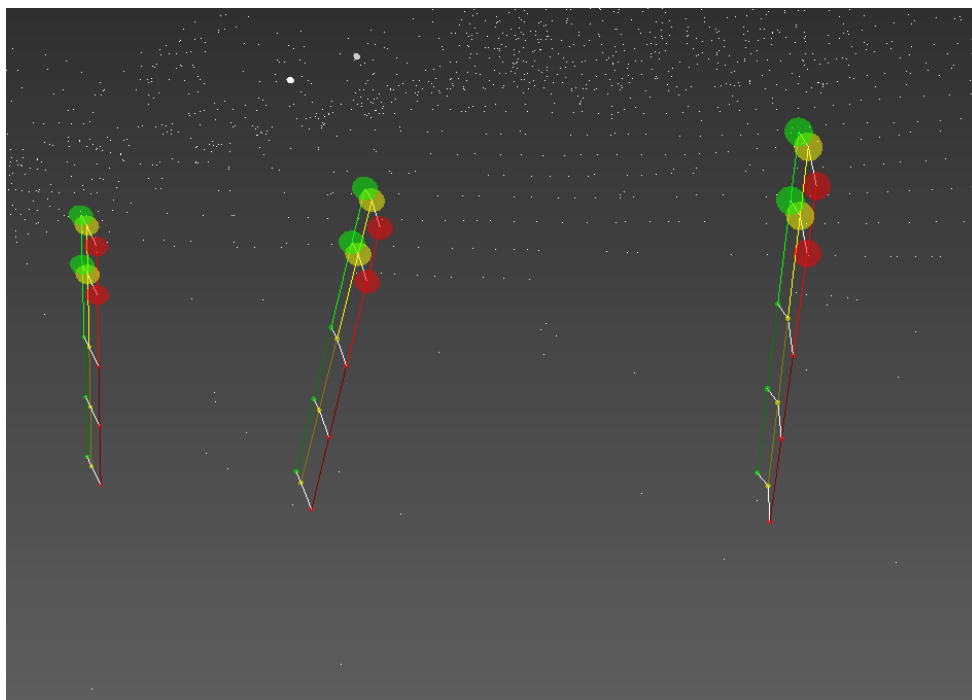


Figure 3.11 Real-World Simulation Scans at Fraternity Circle. (Red Targets Are Initial Position, Yellow Targets Are Intermediate Position, and Green Targets Are Final Position.)

3.10.2. Precision Using the Incremental Displacement Apparatus. The LiDAR Team at Missouri S&T was comparing the resolution of scan data between the three scanner units and needed some way to quantify the scatter. Thanks to Ken Boyko, who fabricated an apparatus that could measure this, the Team was able to make a reasonable comparison. Figure 3.12 shows a photo of the apparatus in action. This same apparatus was used to move a sphere a known distance and compare that measurement with what a LiDAR scan showed. Figure 3.13 is an XYZI point file from a scan of the apparatus. Having a known percentage error afforded some credence to the results of the research for this thesis. Table 3.4 shows the results of a test scan using the apparatus.

Table 3.4 Results From An Initial Test Run of The Incremental Displacement Apparatus

Incremental Displacement Apparatus Results														Δ	
Ball ID:	5	Date:	f1	dist:	255.74	mm	Ball ID:	5	Date:	f2	dist:	255.58	mm	-0.16	mm
Ball ID:	6	Date:	f1	dist:	387.83	mm	Ball ID:	6	Date:	f2	dist:	387.91	mm	0.08	mm
Ball ID:	7	Date:	f1	dist:	332.91	mm	Ball ID:	7	Date:	f2	dist:	333.12	mm	0.21	mm
Ball ID:	8	Date:	f1	dist:	355.07	mm	Ball ID:	8	Date:	f2	dist:	355.12	mm	0.05	mm
Ball ID:	9	Date:	f1	dist:	370.43	mm	Ball ID:	9	Date:	f2	dist:	370.41	mm	-0.02	mm
Ball ID:	10	Date:	f1	dist:	367.49	mm	Ball ID:	10	Date:	f2	dist:	367.46	mm	-0.03	mm
Ball ID:	11	Date:	f1	dist:	263.49	mm	Ball ID:	11	Date:	f2	dist:	263.52	mm	0.03	mm
Ball ID:	12	Date:	f1	dist:	348.83	mm	Ball ID:	12	Date:	f2	dist:	348.97	mm	0.14	mm
Minimum Absolute Value Difference Distance occurred on Rod 9 on date f2: 0.02mm															
Maximum Absolute Value Difference Distance occurred on Rod 7 on date f2: 0.203mm															
Average Absolute Value Difference Distance: 0.09mm															

The data presented in Table 3.4 represents a preliminary test performed before any actual site scans were made. This test was used as a reference for all future scans using the Leica. The results of this test have direct applicability to the research presented in this thesis in that the claim of sub-millimeter precision can be substantiated.



Figure 3.12 Image of Incremental Displacement Apparatus

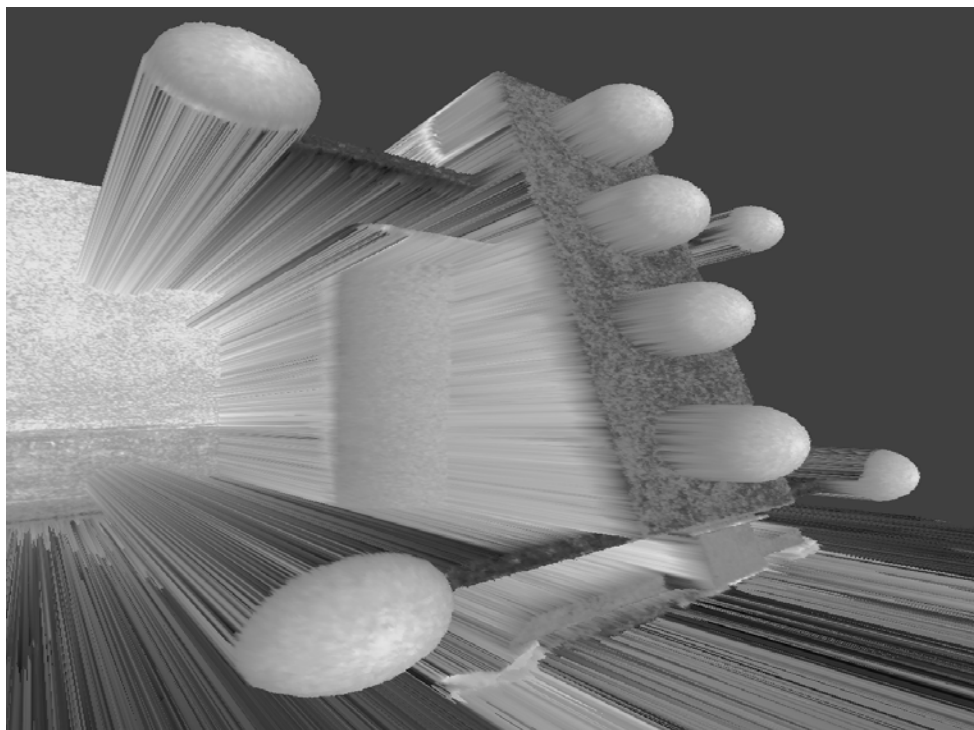


Figure 3.13 Example Scan of Apparatus

4. FINDINGS AND CONCLUSION

The data for this thesis was gathered between July of 2013 and September of 2014. While the schedule was not rigid, every attempt was made to scan after a significant event such as heavy rainfall or extended drought.

4.1. DATA

The data is best represented by visual methods, but, with careful examination of specific points, the general displacement can be deduced.

4.1.1. Point Files. The point files show the clipped, theoretical center points for the spheres in the respective scenes. The output format gives the Ball ID, the ball's role, and the X, Y, Z location.

4.2. DISPLACEMENT VECTORS

The processing software allows for the placement of vectors along the length of each piece of rebar. The reason two balls were used on each floating point target was so that three dimensional displacements could be determined. Having a constant height above ground and a varying depth below ground, the array of floating points allowed for a more complete picture of the morphology of the slide body. The parameters needed to make such a determination were: Diameter of target sphere, Total length of rebar, Height of Rebar above/below ground, Distance between spheres. Figures 4.1 and 4.2 show illustrations of floating point movement with respect to the shear plane. The data is difficult to visualize without a graphical representation, but when the numbers are crunched it illustrates the capabilities of the technique presented in this thesis. To save readers the extra effort, the author solved for the resultant of each vector using ArcGIS.

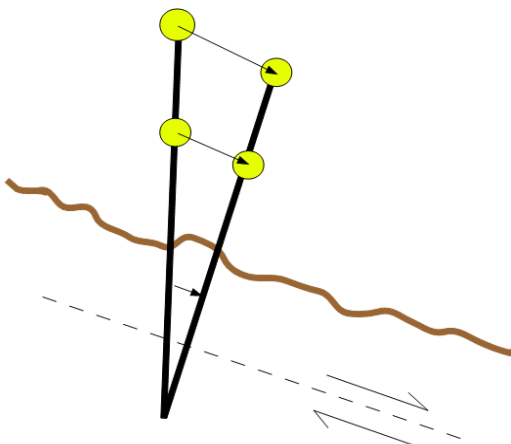


Figure 4.1 Movement of Floating Points That Penetrate Shear Plane

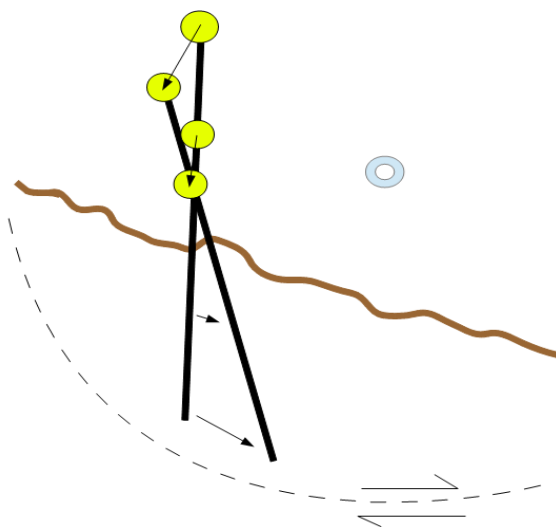


Figure 4.2 Movement of Floating Points That Do Not Penetrate the Shear Plane

4.3. SOURCES OF ERROR

Although every effort to minimize human errors was made, the possibility remains that some mistakes were unavoidable. Before each visit, a plan was reviewed and put in place. The author would visit the site the evening before a scan was scheduled and made sure that there would be no obstructions or issues for the next morning. During each scan, precautions were taken to allow for problem free scanning. In the extreme heat of the summer months, the author would take coolers with extra water, cans with extra gas, and extra weed eater string to prevent a lapse in scanning. After each scan visit, notes were reviewed and updated. At the end of each scan day, before leaving the site, the author would take photos and make sketches, when necessary, and take notes about site conditions, scanning issues, and anything site related that was noteworthy, as well as comparing notes from the previous scan to check for inconsistencies.

Even with every precautionary action taken the author must confess that some mistakes were noticed once a final check was made back at the office in Rolla. Unfortunately, once the data had been collected there was no changing it. The upside is it allowed for on-the-spot improvements to the process of data collection and software utilization.

4.4. RESULTS

A minor amount of movement was detected over the course of this research. The direction and displacement was considered consistent with the style of failure that was occurring. The general displacement is rotating eastward and translating southward where the translation is larger by an order of magnitude. The author explored many different programs to display the resulting morphology, but the results were best-suited using displacement vectors. The research was mainly focused on the movement of the targets so extra data points were not useful for more than aesthetic manipulations. Figures 4.3 and 4.5 show example visualizations of how the movement will be represented. Figure 4.4 is a reference image to allow the viewer to orient the movement in figures 4.5-4.6 and Figure 4.9. Figures 4.6 shows displacement spheres attached to the projected bottom of floating point rods; Red is first date, Yellow is second date, and Green is third date. Displacement vectors connect the sphere centers. Figure 4.7 shows the displacement of

each rod, as viewed from the scanning location. Figure 4.8 shows the displacement of vectors, to scale, in plan view. Figure 4.9 is a profile view of the displacement.

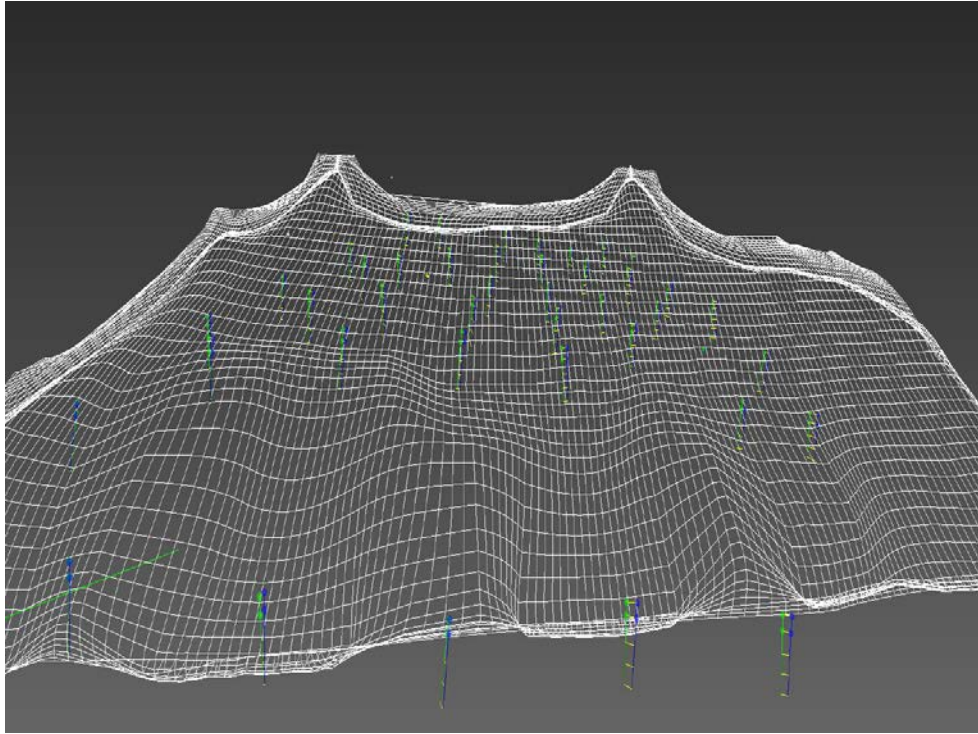


Figure 4.3 Example Grid View of Site Showing Displacement (Green Represents 1st date, Blue Represents 2nd date, Yellow Lines Represent Movement)

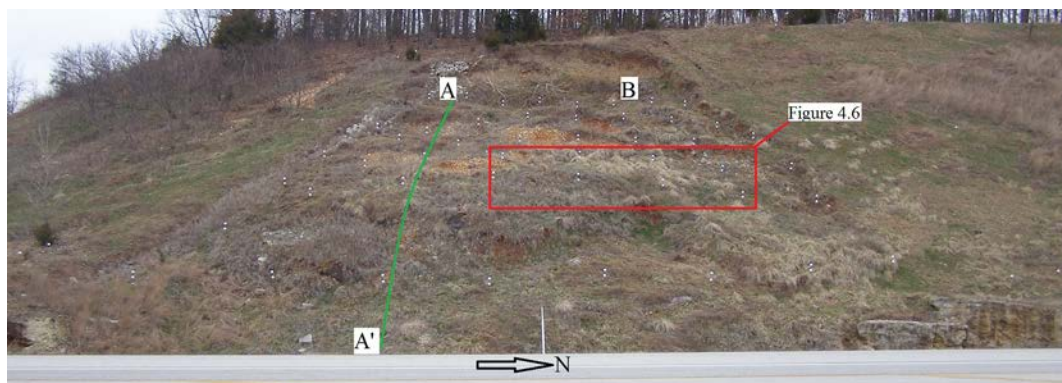


Figure 4.4 Reference Image Showing Location for Figures 4.5, 4.6 and 4.9

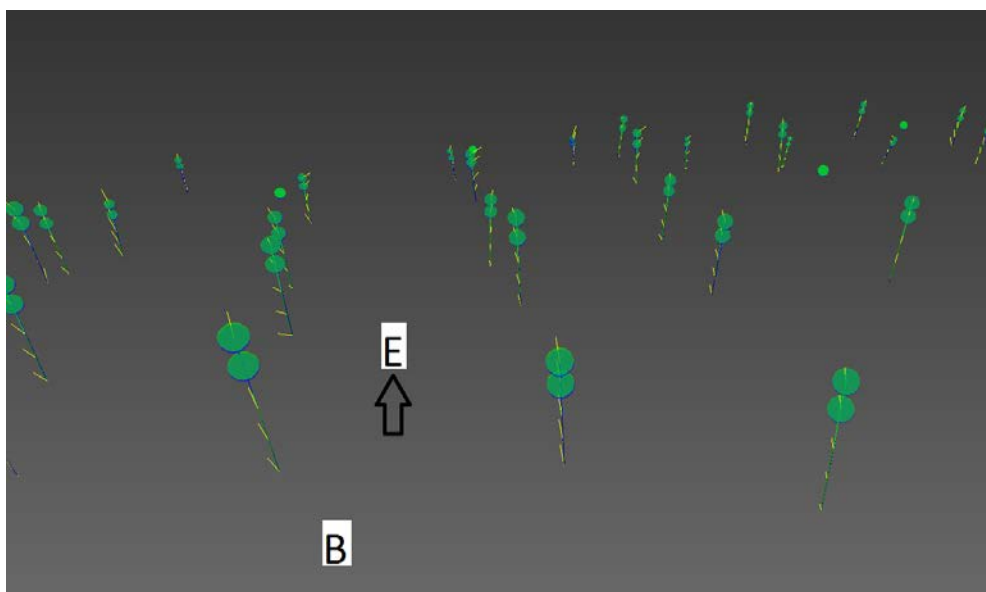


Figure 4.5 Example of a Rotated View of Site Showing Displacement between March and May (Yellow Lines Represent Movement)

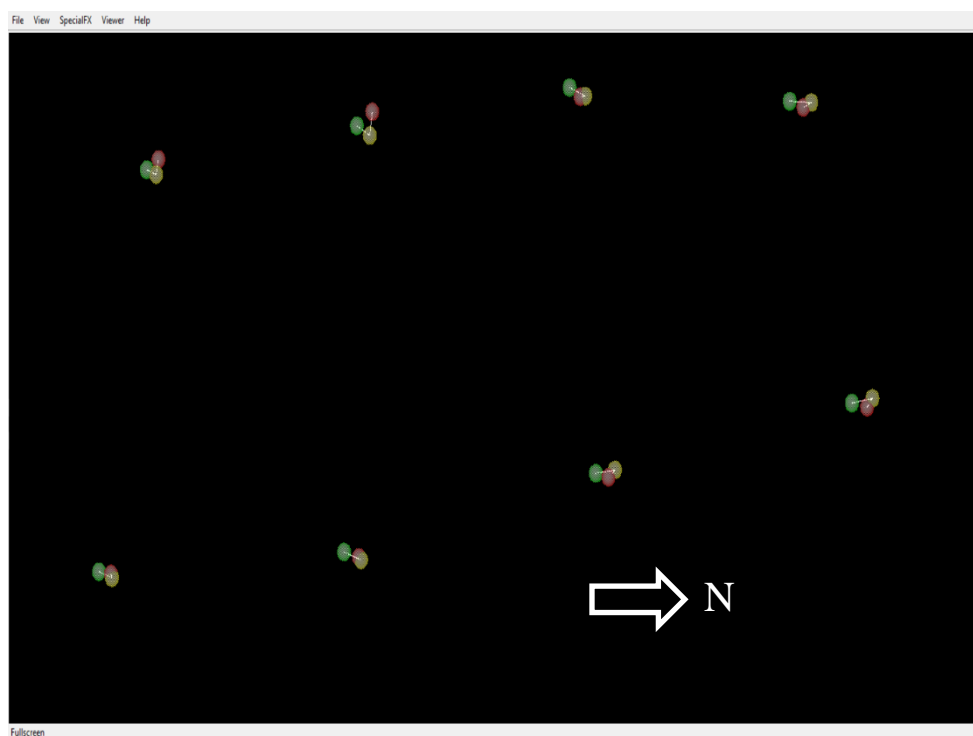


Figure 4.6 Displacement Spheres Attached to the Projected Bottom of Each Rod at the Middle Right Section of Site (Red=Initial, Yellow=Intermediate, Green=Final)

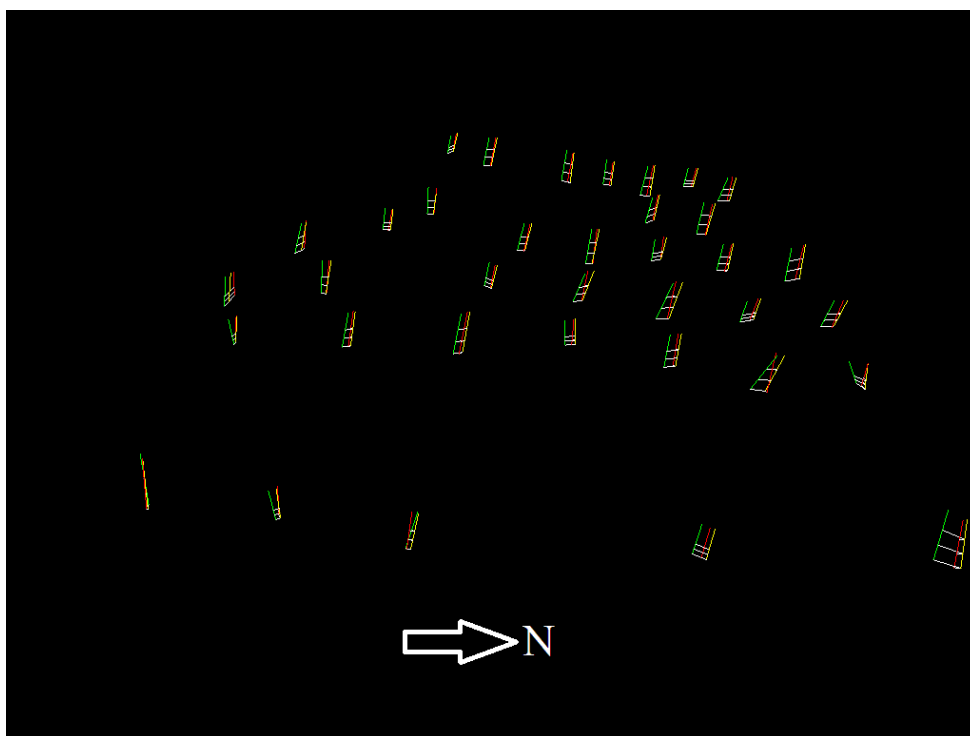


Figure 4.7 Graphical Representation of Vectors at Site Viewed From Scanner Location (Red=Initial, Yellow=Intermediate, Green=Final, Not to Scale)

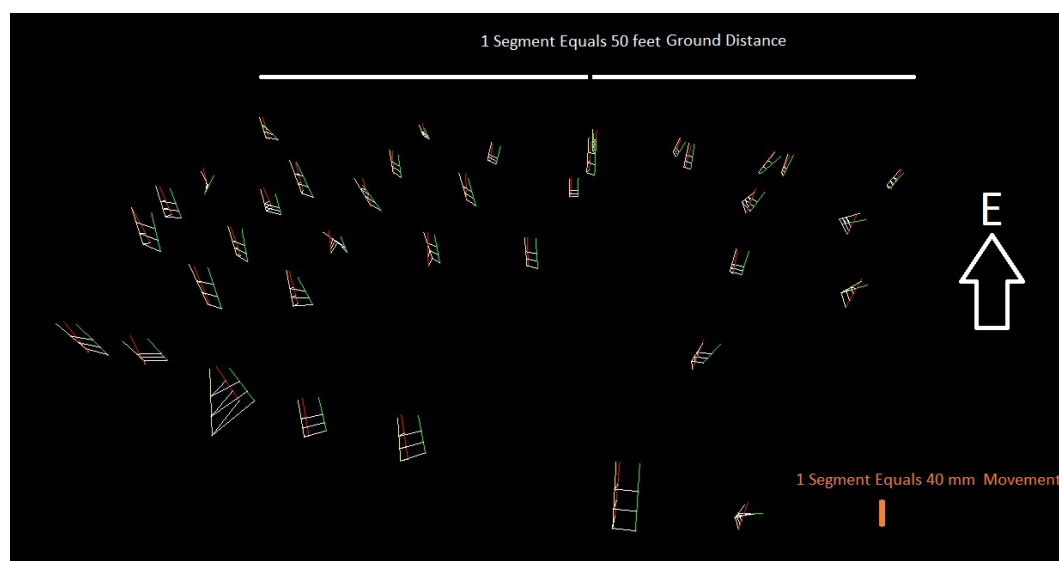


Figure 4.8 Graphical Representation of Vectors (Red=Initial, Yellow=Intermediate, Green=Final)

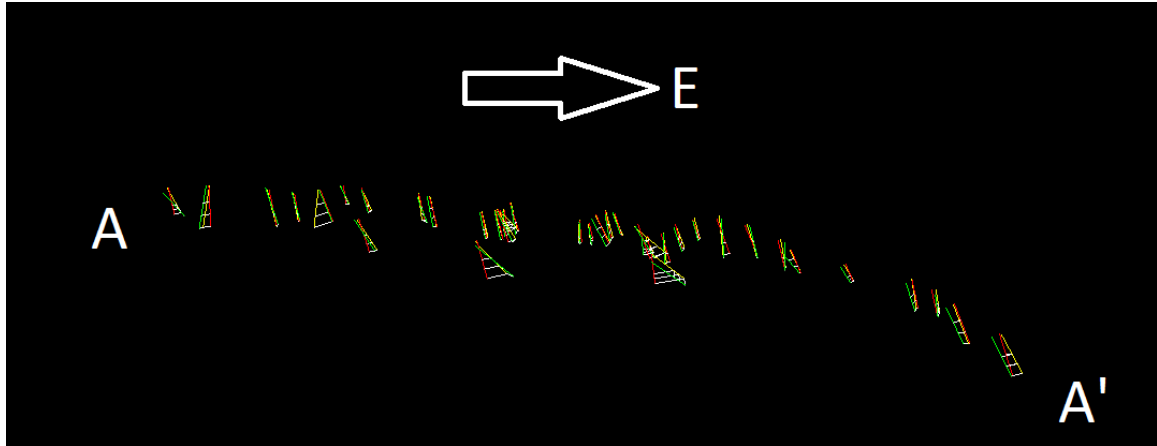


Figure 4.9 Profile View of Slide (Looking North)

4.5. SUGGESTIONS FOR IMPROVEMENT

There are certainly areas with room for improvement in the technique and this research has exposed nearly all of the bugs in the research code used for processing. The author has often been caught up in the potential this research shows and where it could eventually lead. Even though this technique shows promise and the software is working, this process can be considered in the “crawl” phase of development.

The author hopes that someone will pursue this research further and enhance the technique so that someday it may be implemented for the better of society. Below are some of the suggestions the author has compiled given his close involvement with the research:

- Develop a system to allow for rapid target deployment
- Incorporate the vegetation filter process into the sequence of processing
- Test different diameter spheres at varying distances to see what the limits of the technique are
- Try using fewer balls until a critical number can be established
- Install monitoring equipment, like piezometers and rain gauges, and try to correlate movement with natural weather events

4.6. CONCLUSION

The results presented in this thesis are the culmination of more than a year's worth of site visits, scans, collaboration with industry colleagues both domestic and international, and email/in-office collaboration with academic colleagues. The data is not definitive, but does show promise. Given the site conditions, slope complexity, and the prohibitive distance from school the author had to improve the method outlined in this thesis "on-the-fly". The software used for this research was mostly already developed and only had to be refined for this particular project. By the end of this research, the software is nearly completely debugged and close to becoming a turnkey solution. The method has proven to be efficient and has opened the possibilities for further utility. This method could be further enhanced to include real-time monitoring of known active landslide areas to prevent costly accidents.

APPENDIX A.
SYSTEMATIC INSTRUCTIONS FOR GATHERING DATA

1. Preparation is Key

a. Knowing what equipment you will need while in the field is paramount. In addition, knowing what equipment is prone to malfunction will save countless hours of wasted time.

b. The distance your site is away from the office should be directly proportional to the amount of backup equipment you pack.

2. Picking a Scanning Location

a. The setup area should be in a safe location that is as close to perpendicular to the scan site as possible.

b. The scanning distance will dictate the size of targets required.

c. The tripod should be set at a height that can be consistently maintained between scans.

d. Push the legs of the tripod firmly into the ground, if scanning on soil. If on pavement, make sure the legs are situated in a textured area.

e. It is also a good idea to mark the location of each leg of the tripod, if possible.

This will help maintain the scanner's XYZ location between each scan, save some time when using the processing software.

3. Attaching the Tribrach

a. Once the tripod is securely placed on the ground, attach the tribrach with the optical plummet facing the slope.

b. Leveling the tribrach is not entirely necessary, but care should be taken so as not to make the tripod top heavy once the scanner is put in place.

4. Attaching the ScanStation2

a. The female power plug-in should face away from the scan area once it is in place.

If it is put on 180° from this your scan window will need to be adjusted by 180°.

b. Once the scanner is sitting on the tribrach, secure it with the latch on the side of the tribrach.

c. Remove the lens covers and unlock the swivel mechanism on the scanner.

5. Start the generator and plug the scanner's power supply in.

6. Turn on the Dell WorkStation Laptop.

7. Both will take a while to warm up. It is normal for the scanner to make a full 360° rotation while it is warming up.
8. Open the Cyclone program on the laptop.
 - a. If you are starting a new project, go to “Configure” on the toolbar at the top and then to “Databases”. Add a new database.
 - b. If you are returning to an ongoing project you can simply find the folder within the Database and double-click on it.
9. Connect the Ethernet cable to the scanner and computer.
 - a. In Cyclone, go to “Scanners” and select ScanStation2. Find the database you created and create a new project folder. Next, open that folder.
 - b. If you opened an existing project the program should already say it is open.
 - c. The next step is to connect to the scanner. Go to “Scanners”, and select “Connect to Scanner”.
10. There is a status bar at the bottom right of the screen that will show you the connection progress. Once the status bar reaches 100%, the bottom left corner of the screen should say “Connected and Ready”.
11. Now the scanner is ready to capture a scan.
 - a. You should have a good idea of the boundary of your scan area. Draw a window around your entire scan area. (This is assuming you attached the scanner with the optical plummet facing the target area. If not, you will need to shift the window by 180°.)
 - b. There is also a more precise way of inputting the boundaries, but this method is not recommended for the initial scan.
 - c. Once the window is set up, click “Image” at the bottom right side of the Model Space screen.

- d. You may need to repeat step “c” a few times if the brightness is off. If so, you must click on “Image” on the top toolbar and select “Adjust Exposure”. Here you can change the amount of exposure based on the amount of lighting at your scan area.
12. After you capture a suitable image, you can readjust your scan window. Do not rely on the image as an exact representation of your scan area. The camera on the scanner is not perfectly aligned with the laser eye. (Keep this in mind when you are drawing windows around small targets.)
13. You should also have an idea of how fine (or coarse) the scan should be. The next step is to adjust the resolution. There are several preloaded options, but you may also enter a specific point spacing in the vertical and horizontal directions.
14. Before you begin a scan you want to probe the distance so the scanner knows how to apply the resolution that you just set up. The probe distance will be the distance at which the scanner obtains the exact resolution you enter. It will have a finer resolution on objects closer and a coarser resolution on objects farther away.
15. Next, click “Scan”. You can watch the progress bar to see how long the scan should take. You should also keep an eye on the indicator lights located on the base of the ScanStation2, between the power connections.
16. Once the scan is finished the scanner will reset back to 0° and then it is ready for another scan. At this point, you may choose to continue scanning within the same “ScanWorld” in the same project file or you can create a new project file and start over. The scanner may assign a new coordinate system to new project files and ScanWorlds so keep that in mind when changing projects.
17. At the end of the scan day, the first step is to turn the scanner off. This is accomplished by simply powering down the generator and unplugging the scanner. The laptop can also be turned off at this point.
18. Next, you should reattach the lens covers and lock the swivel mechanism.
19. Now the scanner can be placed back into its protective carrying case.
20. The next step is done in the office. To export the data just collected, turn on the Dell WorkStation and open Cyclone.

21. Find the database where you created your new project under the “Servers” directory.
22. Double click through the chain of sub-directories until you find the Model Space you created. When you double click on it, a splash screen will open that scan.
23. From here you can select all of the data or fence the area of interest to minimize the size of the file to be exported.
24. To export all of the available data collected during the scan, including Intensity and RGB, click on “View” and then “View Object As”. Select “Point Cloud” and then “Color Map”. Change the Mode to “Colors from Scanner” then click “Apply”, and “Ok”.
25. Click “File”, then “Export”. Select the desired output directory folder. A common mistake is exporting the files in .PTX format, which is the default for Cyclone. Before you click “OK”, make sure the File Type pull-down says .PTS. Now click “Export”.
26. The new file should be exported in a point format that can be further manipulated using a processing software of your choice.

APPENDIX B.
RESEARCH CODE

Development Environment

All software was developed in-house using C++, running on Ubuntu Linux 10.2 (Lucid Lynx). The GCC (GNU Compiler Collection) was used for compilation. Several standard run-time libraries, such as math.h, stdio.h, and string.h, etc were also employed. Scripting was accomplished using bash (GNU Born Again Shell), copyright by the Free Software Foundation.

Two free external libraries were used for graphic display:

OpenCV – (Open Source Computer Vision Library) Originally developed by Intel, and now supported by Willow Garage. This library is free for use under the open source BSD license.

OpenGL – Registered trademark, Silicon Graphics, Inc.

Directory

The root directory for the processing was kept in the C:\ drive for ease of access. A skeleton template exists from the original software development and each time a new project is run that skeleton template is just copied into a folder named OutCropData. Most of the executable programs write log files that contain details of the processing steps. Each of the empty folders in the skeleton file is built to hold these processed files for later review, or should something go wrong during processing.

Skeleton Template of Data Folders

clippedPointFiles – Clips the point file to only include points around the balls identified (only keeps around 3% of the points - makes the next program run faster).

metadata – Records minimum-maximum extent and set-up information used during initial loading.

pixColorAfterLoad – Displays color images after the initial load executable is run.

pixIntensityAfterLoad – Displays intensity images after the initial load executable is run.

pointFiles – Contains the original point files exported from Cyclone.

regObservations – Contains both the manually picked points and the theoretically calculated sphere centers. This folder also stores the transform values used for

registration between dates. A report on the amount of error and displacement is recorded here as well.

Configuration Files

RodConfig.txt – This file told the processing software how many rods were in the scene, how long each rod was, and whether the rod was used for control points or floating points.

BallSize.txt – This file was a standard file created in preparation for a variance in sphere sizes. It told the processing software the diameter of each sphere in the scene.

Resolution.config – This file is what the processing software used to set up the mesh which controlled how large the scene would be, if the scene contained intensity and color information, if there was a “Z” offset due to setup error, the orientation of the scan site, how many hits to allow per pixel, and what type of coordinate system to use for the projection.

VRMLDateList.txt – This file was used for the final product. It told the processing software what dates to use when comparing before and after scans so that displacement vectors could be drawn.

Naming Convention for Files

The naming convention used was based on “Same Site, Different Date”. The following convention was used:

S yyyy-mm-dd.ext

S: Site number

yyyy: four digit year code

mm: two digit month code

dd: two digit day code

ext: extension (generally .bin, .txt, .config, .png, .pts)

Executable Organization

Each executable file mentioned in 3.8.1. were organized in an external folder named “lidarsw”. Each executable performed a specific operation and was intuitively named to illustrate that operation. The executables were organized as such:

findMinMax.exe: Initial program to determine the extent of data and make that data conform to the desired mesh

load.exe: Secondary program that loaded the meshed data into the pointFiles folder

view2surf.exe: Tertiary program used to locate and identify spheres in the scene

clipSpheres.exe: Tertiary program used to cut down the number of points

findSpheres.exe: A recursive program used to calculate the theoretical center of every sphere in the scene

regballs.exe: Tertiary program used to overlay “after” scans on “before” scans

surf2vrml.exe: Tertiary program used to calculate the amount of displacement that occurred between scan dates and visually display that based on specific commands

APPENDIX C.
DATA TABLES

Theoretical Center for Spheres in Initial Scan

ID	Role	X	Y	Z	ID	Role	X	Y	Z
1	c	-13498	50232	335.87	52	f	9796	69847	9267
2	c	-13248	53756	726.36	53	f	9806	69837	9487
3	c	-3429	68851	7864.7	54	f	9577	45910	-238.2
4	c	1850.6	81241	13340	55	f	9603	45959	-31.74
5	c	3004.3	81353	13773	56	f	9661	53494	3848.3
6	f	-8377	47242	-535.4	57	f	9645	53518	4103.7
7	f	-8372	47257	-331.1	58	f	10228	57128	5134.1
8	f	1.#IND	1.#IND	1.#IND	59	f	10241	57122	5389.9
9	f	-5371	51234	1668.1	60	f	10801	61533	6386.7
10	f	-3295	55718	3597.4	61	f	10795	61539	6595.5
11	f	-3305	55690	3814.6	62	f	11227	65219	7777.7
12	f	-1789	60701	5232.1	63	f	11230	65250	7996.6
13	f	-1792	60701	5464.8	64	f	11917	69645	9022.6
14	f	737.84	65227	7134.1	65	f	11915	69620	9268.7
15	f	742.71	65231	7344.5	66	f	13856	46341	-379.4
16	f	3577.4	70774	9441	67	f	13890	46384	-116.3
17	f	3593.8	70767	9667	68	f	13584	54168	3703.9
18	f	-2978	46571	-456.8	69	f	13580	54174	3956.1
19	f	-3015	46611	-249.2	70	f	13837	57652	5125.5
20	f	-1913	51633	2908.1	71	f	13852	57683	5317.3
21	f	-1918	51631	3164.8	72	f	13806	61859	6370.1
22	f	276.57	55844	4456.8	73	f	13797	61850	6579.7
23	f	273.53	55862	4700.2	74	f	13766	65141	7892.5
24	f	1833	60911	6152.8	75	f	13775	65133	8160.5
25	f	1855.9	60902	6363.5	76	f	13921	69147	9122.1
26	f	3318.5	65135	6933.7	77	f	13938	69176	9357.7
27	f	3318.5	65144	7182.7	80	f	17483	54862	3291.5
28	f	5693.8	70404	9479	81	f	17490	54877	3512.6
29	f	5713.9	70359	9726.5	82	f	17387	58270	4739.4
30	f	1194.7	46031	-563	83	f	17426	58266	4961.7
31	f	1172.3	46037	-320.5	84	f	16879	62100	6347.6
32	f	1946.8	52126	3476.9	85	f	16895	62090	6614.9
33	f	1955.3	52163	3713.7	86	f	16404	65235	7820.2
34	f	1.#IND	1.#IND	1.#IND	87	f	16413	65234	8060.9
35	f	2950.4	55973	5074.8	88	f	16043	68783	9274.6
36	f	4636.1	60053	5816.9	89	f	16066	68764	9515.2

Theoretical Center for Spheres in Initial Scan (Cont.)

37	f	4756.6	61140	6178.7	90	f	21904	47695	398.74
38	f	6042	65299	7427.1	91	f	21901	47726	603.09
39	f	6031.2	65287	7710.7	92	f	21272	55563	3189.9
40	f	7741.1	70147	9062.6	93	f	21271	55538	3435.9
41	f	7767.1	70175	9292.7	94	f	21083	58965	4965.6
42	f	5153	45595	-599	95	f	21115	58936	5207.3
43	f	5158.8	45588	-391	96	f	20046	62100	6749.4
44	f	5832	52766	3833.1	97	f	20057	62113	6971.9
45	f	5849.1	52789	4045.2	98	f	18936	65304	7597.8
46	f	6567.6	56646	4998.7	99	f	18956	65298	7829.8
47	f	6584.5	56654	5214.2	100	f	17888	68466	9123.5
48	f	7822.3	61249	6218.5	101	f	17902	68486	9343.4
49	f	7844.4	61249	6471	102	c	32209	64070	7825.2
50	f	8642.6	65205	7868.8	103	c	27493	82420	16528
51	f	8635.7	65206	8066.4	104	c	29016	84635	17807

Theoretical Center for Spheres in Second Scan

ID	Role	X	Y	Z	ID	Role	X	Y	Z
1	c	-13498	50232.3	335.867	52	f	9796.47	69847.1	9267.04
2	c	-13248.1	53755.5	726.357	53	f	9806.21	69836.7	9487.03
3	c	-3429.48	68850.9	7864.65	54	f	9576.56	45909.5	-238.202
4	c	1850.58	81241	13340.1	55	f	9603.02	45959.2	-31.7407
5	c	3004.27	81352.8	13773.2	56	f	9661.09	53493.5	3848.27
6	f	-8376.88	47241.7	-535.415	57	f	9644.86	53517.8	4103.66
7	f	-8372.15	47256.6	-331.095	58	f	10228.1	57128.3	5134.08
8	f	1.#IND	1.#IND	1.#IND	59	f	10241	57121.6	5389.87
9	f	-5370.73	51234.3	1668.08	60	f	10801.1	61532.8	6386.68
10	f	-3294.96	55718	3597.38	61	f	10795.2	61539.4	6595.52
11	f	-3305.42	55689.8	3814.58	62	f	11227.1	65218.7	7777.73
12	f	-1789.01	60700.9	5232.08	63	f	11229.7	65250.2	7996.57
13	f	-1791.7	60700.7	5464.78	64	f	11917.3	69645.1	9022.55
14	f	737.835	65226.5	7134.13	65	f	11914.8	69619.5	9268.73
15	f	742.709	65231	7344.45	66	f	13855.9	46341.4	-379.351
16	f	3577.39	70773.7	9440.98	67	f	13890.3	46383.6	-116.343
17	f	3593.78	70767.2	9667.04	68	f	13583.5	54167.6	3703.94
18	f	-2978.17	46571	-456.775	69	f	13579.6	54174.4	3956.11
19	f	-3014.73	46611.3	-249.184	70	f	13836.7	57652.2	5125.52
20	f	-1912.62	51632.7	2908.1	71	f	13852.4	57683.3	5317.25
21	f	-1917.55	51630.6	3164.79	72	f	13806.3	61859.1	6370.05

Theoretical Center for Spheres in Second Scan (Cont.)

22	f	276.567	55843.9	4456.81	73	f	13796.8	61850.1	6579.74
23	f	273.526	55862.3	4700.18	74	f	13765.8	65141.4	7892.54
24	f	1833.01	60910.5	6152.8	75	f	13774.7	65132.9	8160.48
25	f	1855.88	60901.9	6363.46	76	f	13920.6	69146.6	9122.1
26	f	3318.53	65135.2	6933.7	77	f	13937.7	69176.3	9357.74
27	f	3318.51	65143.9	7182.66	80	f	17482.5	54861.9	3291.45
28	f	5693.84	70404.3	9478.99	81	f	17489.8	54876.7	3512.56
29	f	5713.93	70359.3	9726.5	82	f	17386.8	58269.6	4739.43
30	f	1194.67	46031.3	-563.001	83	f	17425.7	58265.8	4961.71
31	f	1172.27	46036.6	-320.543	84	f	16878.6	62099.5	6347.6
32	f	1946.8	52125.9	3476.85	85	f	16895.4	62089.8	6614.92
33	f	1955.33	52163.2	3713.66	86	f	16403.7	65234.5	7820.15
34	f	1.#IND	1.#IND	1.#IND	87	f	16413	65234.2	8060.92
35	f	2950.44	55972.9	5074.8	88	f	16043.4	68783	9274.62
36	f	4636.12	60052.7	5816.86	89	f	16066.4	68764.3	9515.21
37	f	4756.6	61139.6	6178.69	90	f	21904	47695.3	398.741
38	f	6041.98	65299.4	7427.12	91	f	21900.9	47725.5	603.09
39	f	6031.15	65287.4	7710.7	92	f	21271.9	55563.1	3189.93
40	f	7741.13	70147.1	9062.61	93	f	21270.7	55538.1	3435.86
41	f	7767.08	70174.7	9292.73	94	f	21082.7	58965	4965.63
42	f	5153	45594.5	-598.997	95	f	21115.4	58935.5	5207.33
43	f	5158.8	45587.9	-391.03	96	f	20045.9	62099.5	6749.44
44	f	5831.96	52765.7	3833.13	97	f	20057.1	62113	6971.88
45	f	5849.05	52788.5	4045.19	98	f	18935.9	65303.9	7597.75
46	f	6567.62	56645.5	4998.74	99	f	18956.2	65297.6	7829.76
47	f	6584.5	56653.7	5214.18	100	f	17887.6	68466.3	9123.54
48	f	7822.26	61248.5	6218.45	101	f	17902.4	68486	9343.37
49	f	7844.36	61249.2	6470.97	102	c	32209.4	64069.6	7825.19
50	f	8642.62	65205.2	7868.76	103	c	27492.8	82419.8	16527.7
51	f	8635.71	65206.3	8066.39	104	c	29015.7	84635.3	17807.4

Theoretical Sphere Centers for Third Scan

ID	Role	X	Y	Z	ID	Role	X	Y	Z
1	c	-23424.2	46224.6	4124.85	52	f	-4625.25	69343	15070.5
2	c	-23898.4	49685.6	4812	53	f	-4615.69	69317.3	15286.3
3	c	-17368.7	65832.7	13314.9	54	f	43.3902.0	46771.8	3643.69
4	c	-14729.5	78521.7	19875.5	55	f	59.3111.0	46817.3	3851.49
5	c	-13624.8	78822.5	20346.4	56	f	-1423.75	53793.7	8332.59
6	f	-17804.5	44425.1	3112.94	57	f	-1447.9	53790.3	8590.52
7	f	-17806.3	44427	3319	58	f	-1593.18	57354	9913.16

Theoretical Sphere Centers for Third Scan (Cont.)

8	f	-15689	48740	5472.02	59	f	-1575.17	57331.7	10167.7
9	f	-15682.9	48734.5	5682.49	60	f	-1937.31	61665.1	11535.8
10	f	-14571.5	53349.8	7994.16	61	f	-1944.4	61657.1	11747
11	f	-14586	53322.5	8208.83	62	f	-2279.57	65237.3	13233.9
12	f	-14100	58396.4	10058.3	63	f	-2284.34	65249.5	13453.8
13	f	-14105.6	58390.3	10292.5	64	f	-2505.08	69585.9	14847.7
14	f	-12556.2	63163.7	12377.9	65	f	-2502.69	69544.5	15087.1
15	f	-12559.4	63158.4	12586.8	66	f	4153.22	48028.5	3630.3
16	f	-10902.4	68982.3	15174.6	67	f	4178.58	48060.2	3895.38
17	f	-10888.9	68968.5	15399.2	68	f	2285.18	55261.9	8312.31
18	f	-12396.1	44863.9	3245.78	69	f	2280.27	55248.5	8565.2
19	f	-12444	44882.1	3453.48	70	f	1837.82	58617.1	10016.8
20	f	-12376.3	49706.1	7017.64	71	f	1849.75	58638.4	10212.4
21	f	-12382.5	49672.9	7269.27	72	f	930.44	62584.9	11590.3
22	f	-11097.1	54145.9	8945.78	73	f	922.926	62562.5	11799.1
23	f	-11107.1	54147.8	9192.25	74	f	231.03	65664.5	13376.7
24	f	-10606.2	59266.4	11076.3	75	f	243.216	65640.1	13638.2
25	f	-10584.4	59244.4	11290.3	76	f	-433.566	69497.8	14935.7
26	f	-10016.6	63620.1	12229.5	77	f	-423.625	69516	15172.9
27	f	-10023.2	63627.2	12474.7	80	f	5990.28	56747.9	8039.26
28	f	-8758.47	69039.9	15226.6	81	f	6004.46	56742.2	8261.34
29	f	-8733.45	68978.3	15472.9	82	f	5166.6	59947.1	9744.88
30	f	-8192.36	45154.9	3158.3	83	f	5203.27	59926.2	9967.4
31	f	-8220.49	45133.7	3398.51	84	f	3891.61	63450.8	11661.4
32	f	-8689.51	50916.7	7700.56	85	f	3909.38	63420.7	11924.5
33	f	-8687.59	50932.1	7942.3	86	f	2783.07	66290.6	13378.8
34	f	-8497.88	54805.4	9376.82	87	f	2791.55	66272.2	13619.5
35	f	-8510.43	54758	9636.74	88	f	1706.68	69556	15097.5
36	f	-7775.32	60118.7	10966.1	89	f	1731.56	69532.5	15334.8
37	f	-7784.07	60078.8	11185.8	90	f	11757.7	50935	4678.39
38	f	-7379.31	64290.5	12789	91	f	11752.8	50955.1	4885.47
39	f	-7391.96	64242	13070.2	92	f	9505.77	58229.6	8066.13
40	f	-6692.56	69231.3	14841.4	93	f	9503.44	58189.9	8311.54
41	f	-6670.64	69239.1	15073.6	94	f	8650.62	61351.9	10109.5
42	f	-4197.84	45561.6	3175.5	95	f	8689.29	61301.7	10349.3
43	f	-4188.08	45540.5	3383.22	96	f	6981.77	64041.2	12106.9
44	f	-5018.77	52300.1	8185.58	97	f	6989.01	64033.9	12332.9
45	f	-5005.31	52300.3	8399.49	98	f	5240.66	66895.3	13196.9
46	f	-5094.1	56156.8	9686.32	99	f	5255.87	66855.7	13429
47	f	-5079.95	56150.4	9899.39	100	f	3591.3	69633.8	14952.5
48	f	-4802.11	60802.9	11287.4	101	f	3604.73	69639.7	15174.6
49	f	-4781.19	60789.2	11543.2	102	c	18494.9	68354.3	13601
50	f	-4813.54	64681.6	13272.6	103	c	10134.1	84598.2	23652.7

Theoretical Sphere Centers for Third Scan (Cont.)

51	f	-4821.34	64653.8	13467.8	104	c	-1.#IND	-1.#IND	-1.#IND
----	---	----------	---------	---------	-----	---	---------	---------	---------

Expression of Displacement Vectors for Each Sphere

ID	x		°	y		°	z		°
1	5.1	cos	72.9	0.4	cos	6.3	0.056	cos	0.9
2	7.5	cos	45	-2.7	cos	16.6	-10.402	cos	60.6
3	-24.06	cos	59.5	-15.3	cos	39.2	11.96	cos	30.9
4	8.99	cos	54.7	8.8	cos	53.6	1.9	cos	12.1
5	11.67	cos	42.8	18.1	cos	63.6	0.5	cos	1.9
6	-0.35	cos	1.4	-19.7	cos	72	3.77	cos	15.2
7	1.57	cos	5.3	-23.5	cos	72.1	4.075	cos	13.8
10	28.18	cos	56.3	16.4	cos	33.9	20.69	cos	42.3
11	33.83	cos	63.1	-5.9	cos	11.7	21.7	cos	42.2
12	19.85	cos	55.9	10.7	cos	31.2	15.6	cos	44.8
13	19.49	cos	58.6	-5.6	cos	17.7	15.45	cos	47.5
14	31.748	cos	68	13.2	cos	30.3	5.45	cos	12.7
15	34.109	cos	70.8	7.9	cos	17.9	6.16	cos	14
16	26.58	cos	66.2	2.9	cos	7.8	13.92	cos	36.7
17	27.12	cos	65	-8.7	cos	22.3	13.3	cos	33.8
18	19.12	cos	37.9	-35.1	cos	65.8	2.472	cos	5
19	21.96	cos	40.1	-37.3	cos	64.8	3.073	cos	5.7
20	16.5	cos	56.2	12.9	cos	44.9	8.54	cos	30.2
21	20.54	cos	53.3	18.2	cos	47.7	11.87	cos	31.7
22	26.036	cos	70.9	-5.4	cos	16.1	5.17	cos	15.4
23	28.297	cos	68.7	-10.8	cos	28.3	4.5	cos	11.9
24	29.54	cos	72.9	-0.9	cos	2.5	2.07	cos	5.7
25	31.12	cos	73	-0.6	cos	1.6	-0.94	cos	2.4
26	37.59	cos	72.9	2.1	cos	4.5	-0.4	cos	0.9
27	39.78	cos	72.7	-3.8	cos	7.7	2.55	cos	5.2
28	35.74	cos	72.2	-0.6	cos	1.3	6.28	cos	14
29	35.32	cos	72	4.3	cos	9.7	5.43	cos	12.2
30	20.75	cos	58.9	1.6	cos	4.8	17.141	cos	49.7
31	25.31	cos	60.7	2.8	cos	7.1	19.068	cos	47
32	15.73	cos	55.8	12.6	cos	45.5	8.18	cos	30.1
33	14.2	cos	49.6	16.4	cos	56.5	5.42	cos	19.5
35	32.49	cos	71.3	-5.4	cos	13	-6.2	cos	14.9
36	-105.22	cos	7.6	-1108.4	cos	72.3	-141.98	cos	10.2
37	25.75	cos	71.4	-5.9	cos	18	-2.29	cos	7

Expression of Displacement Vectors for Each Sphere (Cont.)

38	35.44	cos	72.4	3.5	cos	7.9	-4.18	cos	9.4
39	40.85	cos	70.9	11.3	cos	21.4	-2.05	cos	3.9
40	27.21	cos	71.3	6.8	cos	19.5	-1.53	cos	4.4
41	25.27	cos	64.6	14.8	cos	39.8	-3.6	cos	9.9
42	-11.93	cos	34.2	-23.2	cos	63.2	9.576	cos	27.6
43	-15.48	cos	40.7	-24.3	cos	61.4	8.86	cos	23.6
44	20.94	cos	65	10.8	cos	35.4	5.81	cos	19.3
45	20.69	cos	58.4	17.1	cos	49.2	4.19	cos	12.5
46	24.13	cos	69.5	-6.4	cos	20.1	-6.21	cos	19.5
47	24.04	cos	69.4	-7.6	cos	23.8	-4.88	cos	15.4
48	26.16	cos	72.7	-2.1	cos	6.5	2.12	cos	6.5
49	25.07	cos	73	-0.9	cos	2.9	0.29	cos	0.9
50	37.22	cos	71.5	8.5	cos	17.9	-2.89	cos	6.1
51	40.1	cos	66.3	20.8	cos	36.5	-4.36	cos	7.8
52	33.72	cos	71.2	2.9	cos	6.7	-8.42	cos	19.5
53	33.91	cos	72.3	0.3	cos	0.7	-5.43	cos	12.8
56	29.33	cos	70.3	-4.6	cos	12.1	8.32	cos	21.7
57	32.2	cos	71.8	-2.9	cos	7.1	6.33	cos	15.5
58	14.2	cos	56.6	-4.3	cos	18	12.39	cos	50
59	9.2	cos	43.2	-3.4	cos	16.3	13.63	cos	61.7
60	23.5	cos	72.5	-2.8	cos	9.5	1.89	cos	6.4
61	21.9	cos	69.9	-6.7	cos	23.2	3.65	cos	12.7
62	32.1	cos	72.2	-5	cos	12.4	-2.41	cos	6
63	32.1	cos	72.4	-2.7	cos	6.7	-3.96	cos	9.9
64	34.6	cos	71.4	5.5	cos	12.5	-6.5	cos	14.7
65	34.4	cos	71.9	3	cos	6.9	-6.36	cos	14.6
66	18.4	cos	41.5	-29.5	cos	63.6	4.622	cos	10.7
67	16.4	cos	34.7	-33.5	cos	66.6	5.279	cos	11.3
68	27.3	cos	64	-10.3	cos	25.7	13.73	cos	34
69	26.3	cos	63.1	-11.6	cos	29.5	13	cos	32.9
70	10.1	cos	28.1	-23.2	cos	61.3	13.73	cos	37.9
71	5.4	cos	15.2	-24.8	cos	64.9	13.58	cos	37.5
72	37	cos	67.6	3.4	cos	6.7	17.02	cos	33.2
73	35.3	cos	67.8	-3.6	cos	7.5	15.75	cos	32.4
74	25.1	cos	67.3	-1	cos	2.9	12.04	cos	34.5
75	22.3	cos	61.6	-5.5	cos	16.1	15.2	cos	43.5
76	28	cos	72.1	3.8	cos	10.8	3.59	cos	10.2
77	26.9	cos	72.3	3.3	cos	9.8	3	cos	8.9
80	5.8	cos	44.3	6.3	cos	47.8	5.76	cos	44
81	-2.5	cos	14.1	13.1	cos	68.3	5.11	cos	28.7
82	40	cos	68.6	-6.1	cos	11.4	15.59	cos	28.8
83	42.3	cos	68.2	-4	cos	7	18.17	cos	31.4
84	35.5	cos	72.2	-5.8	cos	13	2.21	cos	5

Expression of Displacement Vectors for Each Sphere (Cont.)

85	37.1	cos	72.5	-1.7	cos	3.7	4.72	cos	10.2
86	40.2	cos	72.5	-3	cos	6	-4.52	cos	9
87	40.2	cos	72.7	-1.4	cos	2.8	-4.36	cos	8.7
88	41.6	cos	72.3	5	cos	9.6	4.31	cos	8.3
89	40.9	cos	72.8	-0.6	cos	1.2	3.78	cos	7.5
90	22.9	cos	30.3	-56	cos	68.7	-2.707	cos	3.6
91	17.1	cos	21.3	-62.3	cos	71	-2.265	cos	2.8
92	43	cos	54.7	-37.7	cos	48.6	20.5	cos	27.1
93	59.1	cos	65.1	-33.4	cos	38.8	8.15	cos	9.6
94	38.7	cos	72.8	-0.9	cos	1.9	3.63	cos	7.6
95	38	cos	72.4	1	cos	2.1	5.63	cos	11.9
96	51.5	cos	69.7	6.1	cos	9	17.56	cos	25.8
97	53.8	cos	70	10.1	cos	14.3	15.56	cos	22
98	53	cos	72.2	-1.8	cos	2.7	8.99	cos	13.5
99	58.2	cos	72.2	6.4	cos	8.8	7.72	cos	10.6
100	28.6	cos	69.8	4.7	cos	12.5	9.03	cos	23.9
101	24.6	cos	68.5	4.9	cos	14.8	9.22	cos	27.7
103	-9.3	cos	52.7	-8.7	cos	49.5	-5.1	cos	29.8

Total Resultant Vector for Each Sphere

Ball ID	Resultant (mm)	Angle	Ball ID	Resultant (mm)	Angle
1	5.1157	-175.5154	52	26.4325	-156.1211
2	7.9712	160.2011	53	33.9113	-179.4931
3	28.5127	32.4527	56	29.6885	171.0866
4	12.5801	-135.6119	57	23.6580	-123.6229
5	21.5360	-122.8120	58	4.9578	-41.7295
6	19.7031	88.9822	59	9.8082	159.7174
7	6.4980	132.3805	60	23.6662	173.2053
10	32.6048	-149.8017	61	18.0056	-167.8163
11	21.2894	146.3398	62	32.4871	171.1466
12	22.5502	-151.6734	63	32.2134	175.1920
13	20.1175	-148.5380	64	35.0344	-170.9679
14	29.4320	-173.3664	65	34.5306	-175.0159
15	35.0119	-166.9596	66	34.7679	121.9530
16	10.9532	168.4131	67	37.2989	116.0842
17	28.4813	162.2139	68	29.1784	159.3290
18	39.9698	118.5784	69	23.6603	171.4932
19	18.1987	-16.6027	70	25.3032	113.5257
20	20.9442	-141.9811	71	25.3811	102.2840
21	15.8273	-136.9714	72	37.1559	-174.7497

Total Resultant Vector for Each Sphere (Cont.)

22	26.5901	168.2827	73	28.0644	168.4899
23	26.4153	-150.5188	74	13.7317	-167.3807
24	11.4918	-135.8814	75	22.9682	166.1453
25	31.1258	178.8955	76	28.1603	110.3655
26	37.6486	-176.8024	77	27.1017	-173.0061
27	39.0915	-163.9620	80	8.5633	-132.6338
28	35.7450	179.0382	81	13.3364	-79.1956
29	35.5808	-173.0587	82	3.4059	176.6335
30	20.8116	-175.5907	83	42.4887	174.5980
31	7.0945	-76.5514	84	21.8195	-158.4912
32	20.1542	-141.3047	85	37.1389	177.3764
33	21.6933	-130.8878	86	30.9196	177.9612
35	32.9357	170.5634	87	40.2244	178.0054
37	26.3651	125.3659	88	25.4562	-134.6817
38	35.6124	-174.3598	89	40.9044	179.1595
39	26.0366	160.9457	90	60.5013	112.2411
40	12.8180	86.9590	91	32.5220	127.5041
41	29.2850	-149.6436	92	57.1864	138.7575
42	26.0876	62.7867	93	67.8850	150.5273
43	28.8118	57.5014	94	30.9571	-99.8579
44	6.7417	122.2756	95	38.0132	-178.4926
45	26.8419	-140.4267	96	42.7355	175.4368
46	17.3466	114.3783	97	54.7398	-169.3675
47	25.2127	162.4562	98	39.9712	-161.4744
48	3.3736	151.6877	99	58.5508	-173.7246
49	25.0861	177.9440	100	17.7505	123.5110
50	38.1782	-167.1359	101	25.0833	-168.7349
51	31.7940	-162.4256	103	12.7350	43.0908

BIBLIOGRAPHY

- Abellan, A, M Jaboyedoff, T Oppikofer, and J M. Vilaplana. "Detection of millimetric deformation using a terrestrial laser scanner: experiment and application to a rockfall event." *Natural Hazards and Earth System Sciences* 9 (2009): 365-72.
- Dunning, S A., C I. Massey, and N J. Rosser. "Structural and geomorphological features of landslides in the Bhutan Himalaya derived from Terrestrial Laser Scanning." *Geomorphology* 103 (2008): 17-29.
- Garcia, A, A Hordt, and M Fabian. "Landslide monitoring with high resolution tilt measurements at the Dollendorfer Hardt landslide, Germany." *Geomorphology* 120 (2009): 16-25.
- Gordon, Stuart, Derek Lichti, and Mike Stewart. "Application of a high-resolution, ground-based laser scanner for deformation measurements." *Proceedings of 10th International FIG Symposium on Deformation Measurements*. 2001.
- Hsiao, K. H., et al. "Change detection of landslide terrains using ground-based LiDAR data." *XXth ISPRS Congress, Istanbul, Turkey, Commission VII, WG. Vol. 7. No. 5*. 2004.
- Kilian, Johannes, Norbert Haala, and Markus Englich. "Capture and evaluation of airborne laser scanner data." *International Archives of Photogrammetry and Remote Sensing* 31 (1996): 383-388.
- Lichti, Derek D., and Sonam Jamtsho. "Angular resolution of terrestrial laser scanners." *The Photogrammetric Record* 21.114 (2006): 141-160.
- Prokop, A., and H. Panholzer. "Assessing the capability of terrestrial laser scanning for monitoring slow moving landslides." *Natural Hazards and Earth System Science* 9.6 (2009): 1921-1928.
- Teza, Giordano, Arianna Pesci, Rinaldo Genevois, and Antonio Galgaro. "Characterization of landslide ground surface kinematics from terrestrial laser scanning and strain field computation." *Geomorphology* 97 (2007): 424-37.
- Wehr, Aloysius, and Uwe Lohr. "Airborne laser scanning-an introduction and overview." *Photogrammetry and Remote Sensing* 54 (1999): 68-82.

How Does Laser Scanning Work. Kemp Design, <<http://floridalaserscanning.com/3d-laser-scanning/how-does-laser-scanning-work/>>. Accessed 1 Feb. 2015.

Mountain Risks. University of Caen Lower Normandy, <<http://www.unicaen.fr/mountainrisks/spip/spip.php?article35>>. Accessed 1 Feb. 2015.

VITA

Nathan Bradley Rohrbaugh was born in Oakland, Maryland and raised on his family farm in Burlington, West Virginia. He joined the Army right out of high school and, by the end of his first enlistment, he decided to become a career soldier. He was injured in combat the night before his scheduled second reenlistment in Iraq. This ended his career in the military and began his path into academia. He earned his Associate of Arts and Science degree in Geology from Potomac State College of West Virginia University in Keyser, West Virginia in May 2008. After finishing his Associate's degree, Nathan started his Bachelor's degree in Geology at Marshall University in Huntington, West Virginia. He finished his Bachelor's degree in December 2011 and started graduate work at Marshall University. During the spring of 2012, Nathan decided to apply to a Geological Engineering program with the intent of gaining credentials as both a professional geologist and a professional engineer. Missouri University of Science and Technology's Geological Engineering program proved to be his best choice.

Nathan worked as both a Graduate Research Assistant and Graduate Teaching Assistant during his time at Rolla. The experience gained as a GRA directly lead to his knowledge of the Leica ScanStation2 and the overall success of his thesis research. He was GTA for labs in Geology for Engineers (GE50), Principles of GIS (GE342), and Physical Mineralogy/Petrology (GLY125). Nathan earned his Master's degree at Missouri University of Science and Technology in May of 2015.